Article:
Moss, C.E., Johnston, S.A., Kimble, J.V. et al. (9 more authors) (2024) Aging-related defects in macrophage function are driven by MYC and USF1 transcriptional programs. Cell Reports, 43 (4). 114073. ISSN 2211-1247

https://doi.org/10.1016/j.celrep.2024.114073

Cell Reports

Article

Aging-related defects in macrophage function are driven by MYC and USF1 transcriptional programs

Graphical abstract

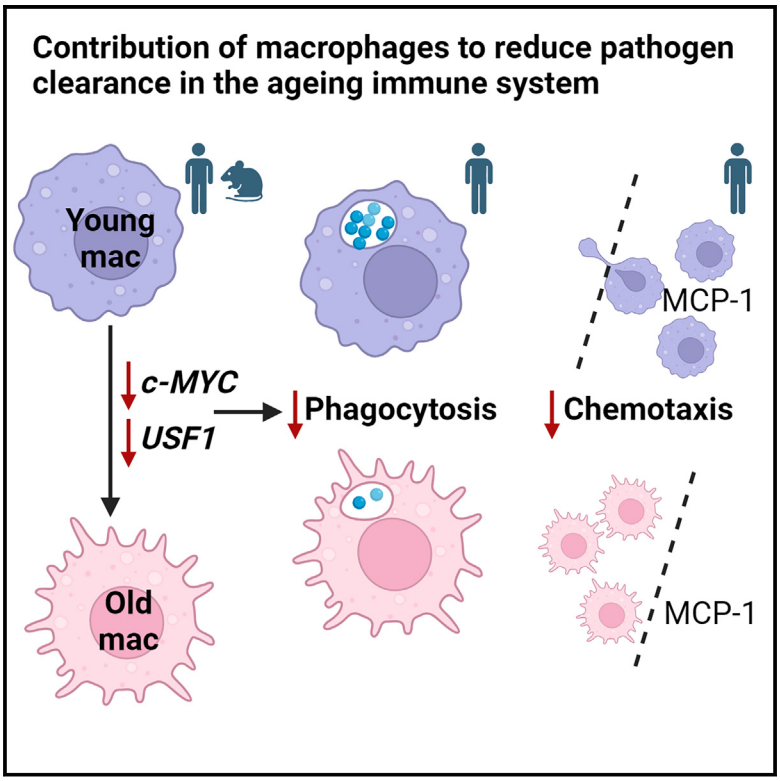

Highlights

- Human monocyte and macrophage migration and phagocytosis is markedly reduced with age
- MYC and USF1 are driving this aged macrophage phenotype in both human and murine cells
- MYC- and USF1-regulated pathways are potential targets for therapeutic intervention

Authors

Charlotte E. Moss, Simon A. Johnston, Joshua V. Kimble, ..., Daniel Coca, Heather L. Wilson, Endre Kiss-Toth

Correspondence

h.l.wilson@sheffield.ac.uk (H.L.W.), e.kiss-toth@sheffield.ac.uk (E.K.-T.)

In brief

Moss et al. report that human monocytes and monocyte-derived macrophages have a marked reduction in migration and phagocytosis. This aged macrophage phenotype is driven by master-regulator transcription factors MYC and USF1 in both human and murine cells, providing a strong platform for identification of pathways and targets for intervention studies.

Moss et al., 2024, Cell Reports *43*, 114073
April 23, 2024
https://doi.org/10.1016/j.celrep.2024.114073

CellPress

Cell Reports

CellPress
OPEN ACCESS

Article

Aging-related defects in macrophage function are driven by MYC and USF1 transcriptional programs

Charlotte E. Moss,[1,2] Simon A. Johnston,[1] Joshua V. Kimble,[1,2] Martha Clements,[1] Veryan Codd,[3,4] Stephen Hamby,[3,4] Alison H. Goodall,[3,4] Sumeet Deshmukh,[5] Ian Sudbery,[5] Daniel Coca,[2,6] Heather L. Wilson,[1,2,*] and Endre Kiss-Toth[1,2,7,8,*]

[1]Division of Clinical Medicine, School of Medicine and Population Health, University of Sheffield, Sheffield, UK
[2]Healthy Lifespan Institute, University of Sheffield, Sheffield, UK
[3]Department of Cardiovascular Sciences, University of Leicester, Leicester, UK
[4]National Institute for Healthcare Research, Leicester Biomedical Research Centre, Glenfield Hospital, Leicester, UK
[5]School of Biosciences, University of Sheffield, Sheffield, UK
[6]Department of Autonomic Control and Systems Engineering, University of Sheffield, Sheffield, UK
[7]Biological Research Centre, Szeged, Hungary
[8]Lead contact
*Correspondence: h.l.wilson@sheffield.ac.uk (H.L.W.), e.kiss-toth@sheffield.ac.uk (E.K.-T.)
https://doi.org/10.1016/j.celrep.2024.114073

SUMMARY

Macrophages are central innate immune cells whose function declines with age. The molecular mechanisms underlying age-related changes remain poorly understood, particularly in human macrophages. We report a substantial reduction in phagocytosis, migration, and chemotaxis in human monocyte-derived macrophages (MDMs) from older (>50 years old) compared with younger (18–30 years old) donors, alongside downregulation of transcription factors MYC and USF1. In MDMs from young donors, knockdown of MYC or USF1 decreases phagocytosis and chemotaxis and alters the expression of associated genes, alongside adhesion and extracellular matrix remodeling. A concordant dysregulation of MYC and USF1 target genes is also seen in MDMs from older donors. Furthermore, older age and loss of either MYC or USF1 in MDMs leads to an increased cell size, altered morphology, and reduced actin content. Together, these results define MYC and USF1 as key drivers of MDM age-related functional decline and identify downstream targets to improve macrophage function in aging.

INTRODUCTION

Macrophages are a critical component of the cell-mediated immune system and act as both regulatory and effector cells in healthy and disease contexts. Macrophages have diverse functions at the interface of the innate and adaptive immune systems, including chemotaxis and migration through tissues, phagocytosis of pathogens and other foreign material, clearance of dead, dying, and senescent cells, and cytokine production.[1] Many subtypes of macrophages exist, depending on tissue environment, differentiation, and activation. The typing of macrophages into pro-inflammatory (M1) and anti-inflammatory (M2) has been invaluable in understanding their biological function *in vitro*. However, much work has also gone into understanding tissue-resident macrophage function, showing that the M1 and M2 classification is much too simplistic for *in vivo* studies. Macrophages exhibit versatility in different settings, and nomenclature should focus on stimulating agents or macrophage function.[2]

Macrophages have been demonstrated to have a key role in inflammaging, the chronic, sterile inflammatory phenotype well studied in aging research,[3] and have been implicated in functional immune decline with age and age-related diseases such as atherosclerosis, diabetes, fibrosis, immunocompromise, autoimmunity, and cancer.[4] It is thought that macrophages become chronically activated with age, with their function more closely resembling an inflammatory macrophage phenotype, including increased inflammatory and stress responses.[5] However, most of our current knowledge in this context relies on mouse models, with a notable lack of studies in humans.[6] How the molecular changes that determine the chronic inflammatory phenotype translate to a decline in function is unclear, creating a critical gap limiting the development of new immunotherapeutics for aging. Here, we sought to measure aging-related changes in monocyte and monocyte-derived macrophage (MDM) migration and phagocytosis in a human cohort as a phenotypic marker to identify the molecular changes underlying macrophage aging.

Age-related changes in phagocytosis and chemotaxis have been reported in several contexts in the literature. Aged mouse peritoneal macrophages show reduced phagocytosis of apoptotic neutrophils,[7] fluorescent particles,[8] and myelin

fragments.[9] In contrast, phagocytosis of zymosan particles was found to be similar between young and old animals,[10] while an earlier study found that phagocytosis activated by adjuvants occurred equally across different age groups.[11] Studies of brain-resident macrophages (microglia) revealed that uptake of myelin[9,12] and lipid debris[13] were reduced with age. Similarly, alveolar macrophages consistently show a reduction in phagocytic activity with age, including lower phagocytosis of apoptotic neutrophils[14] and *Escherichia coli*.[15] Finally, aged mouse bone marrow-derived macrophages (BMDMs) showed no defect in uptake of zymosan,[10] fluorescent,[8] latex,[16] or *E. coli* particles[17] but decreased phagocytosis with age in uptake of apoptotic Jurkat cells,[18] myelin fragments,[9] and apoptotic N2A cell debris or *E. coli* bioparticles.[19] The effect of age on phagocytosis in human monocytes or MDMs has not yet been assessed.

Mouse peritoneal macrophages and BMDMs showed improved chemotaxis with age, including toward the chemoattractants *N*-formyl-methionyl-leucyl-phenylalanine[20] and C-C motif chemokine ligand 2 (CCL2).[21] Contrastingly, aged BMDMs had slower migration toward an implanted polypropylene mesh surface.[17] Therefore, the effects of aging on macrophage phenotype were dependent on the environment and nature of stimulus.

Few publications have studied the effects of aging on cell migration in humans. Aged human granulocyte macrophage colony-stimulating factor-derived MDMs showed preferential migration toward conditioned media from immune senescent cells.[22] The early macrophage response in human macrophages to pro-inflammatory stimuli such as lipopolysaccharide (LPS) is well understood and utilized in both *in vivo* and *in vitro* models. Macrophages from older animals have tissue-specific alterations in pro-inflammatory responsiveness to LPS.[23] Although LPS induces a predominantly M1 phenotype, more varied phenotypes may exist *in vivo*, and other phenotypic changes and stimuli have been less studied.

Transcription factor (TF) analysis has been key in interpreting macrophage biology and function, but so far it has only been used in a small number of studies that focused on inflammaging. In aged murine macrophages, loss of Krüppel-like factor 4 (KLF4) has been attributed to loss of diurnal rhythmicity of phagocytosis with age.[24] TF regulons were used to predict that KLF4 and interferon regulatory factor 5 were decreased with age in tissue macrophage populations. This was associated with a trend to a switch from an M1-like to an M2-like macrophage phenotype, known to occur in age-related tumor growth promotion.[25] Older alveolar macrophages have been found to have a "senescent-like" phenotype with reduced proliferation, insensitivity to growth factor stimulation, and increased p16 and senescence-associated secretory phenotype components. Core binding factor β (CBFβ) was found to be lost in these aged cells and preferentially present in proliferating cells, indicating that CBFβ deficiency might push alveolar macrophages toward senescence.[26]

Overall, current knowledge indicates dysregulation of macrophage function with age that could be tissue and/or stimulus specific. It has previously been reported (mostly using murine cells) that macrophages undergo functional decline with age, including a reduction in phagocytosis and chemotaxis.[17,19] However, there is a lack of consensus as to whether and to what extent this also occurs in primary human macrophages. Additionally, the underlying mechanisms driving these age-related changes are largely unknown. We therefore investigated the impact of aging on primary human MDM function to characterize intrinsic, age-related changes to macrophage function and reveal the molecular mechanisms that underpin these changes. We found that aging significantly reduced macrophage function and altered morphology. This age-related dysfunction and the morphological changes were replicated with knockdown of either *MYC* or *USF1* (two TFs with reduced expression in aged macrophages) in MDMs isolated from young donors. Finally, we identified key transcriptional targets downstream of *MYC* and *USF1* with age-related dysregulated expression that may be driving age-dependent changes in macrophage morphology and function.

RESULTS

Human MDM function is reduced with age

Monocytes were isolated from healthy volunteer blood from two gender-balanced groups: aged 18–30 years (mean age 23.7 ± 1.2 years; young cohort) or >50 years (mean age 60.5 ± 5.7 years; older cohort). Monocytes were either used directly in functional assays or differentiated into MDMs. Further information on demographics of human donors can be found in Table S1.

Functional assays were then performed in freshly isolated blood monocytes, resting (M^0) MDMs, or MDMs activated for 24 h with LPS and interferon-γ (IFN-γ) stimulation ($M^{LPS+IFN\gamma}$ MDMs) (Figure 1). The phagocytic capacity of monocytes and MDMs was assessed by the uptake of opsonized fluorescent beads (Figures 1A and 1B) and/or fluorescent *Staphylococcus aureus*, measured as the mean fluorescence intensity, indicative of the number of beads/bacteria taken up by each cell (Figures 1C–1E).

MDMs from older humans had severely reduced phagocytic capacity compared to cells isolated from young donors (Figures 1A–1C). Compared to the cells from the younger subjects, phagocytosis in M^0 MDMs from older subjects was reduced by 35% ($p < 0.05$) and by 42% ($p < 0.05$) in older $M^{LPS+IFN\gamma}$ MDMs. In young cells, $M^{LPS+IFN\gamma}$ MDMs showed 30% ($p < 0.05$) reduction in phagocytosis compared with M^0. Similarly, older monocytes exhibited reduced phagocytosis of both beads (Figure 1D) and *S. aureus* (Figure 1E), suggesting that this phenotype is maintained throughout the *in vitro* differentiation to MDMs. Older $M^{LPS+IFN\gamma}$ MDMs also showed a slight reduction in phagocytosis compared with M^0 MDMs of the same age. However, this change was not statistically significant, as mean fluorescence in older M^0 MDMs was already reduced to levels similar to those in young $M^{LPS+IFN\gamma}$ MDMs (mean ± SEM: 24.46 ± 3.93 vs. 26.23 ± 2.08) (Figure 1C).

Cell migration in M^0 MDMs was significantly reduced in older donors compared to young counterparts (89% less migration in macrophages from older compared to young after 14-h migration in a scratch wound assay; $p < 0.01$). Compared to the M^0 MDMs, migration of $M^{LPS+IFN\gamma}$ MDMs in the young group was much lower (98% reduction after 14 h; $p = 0.0021$) but was comparable in both M^0 MDMs and $M^{LPS+IFN\gamma}$ MDMs in the older group (Figure S1).

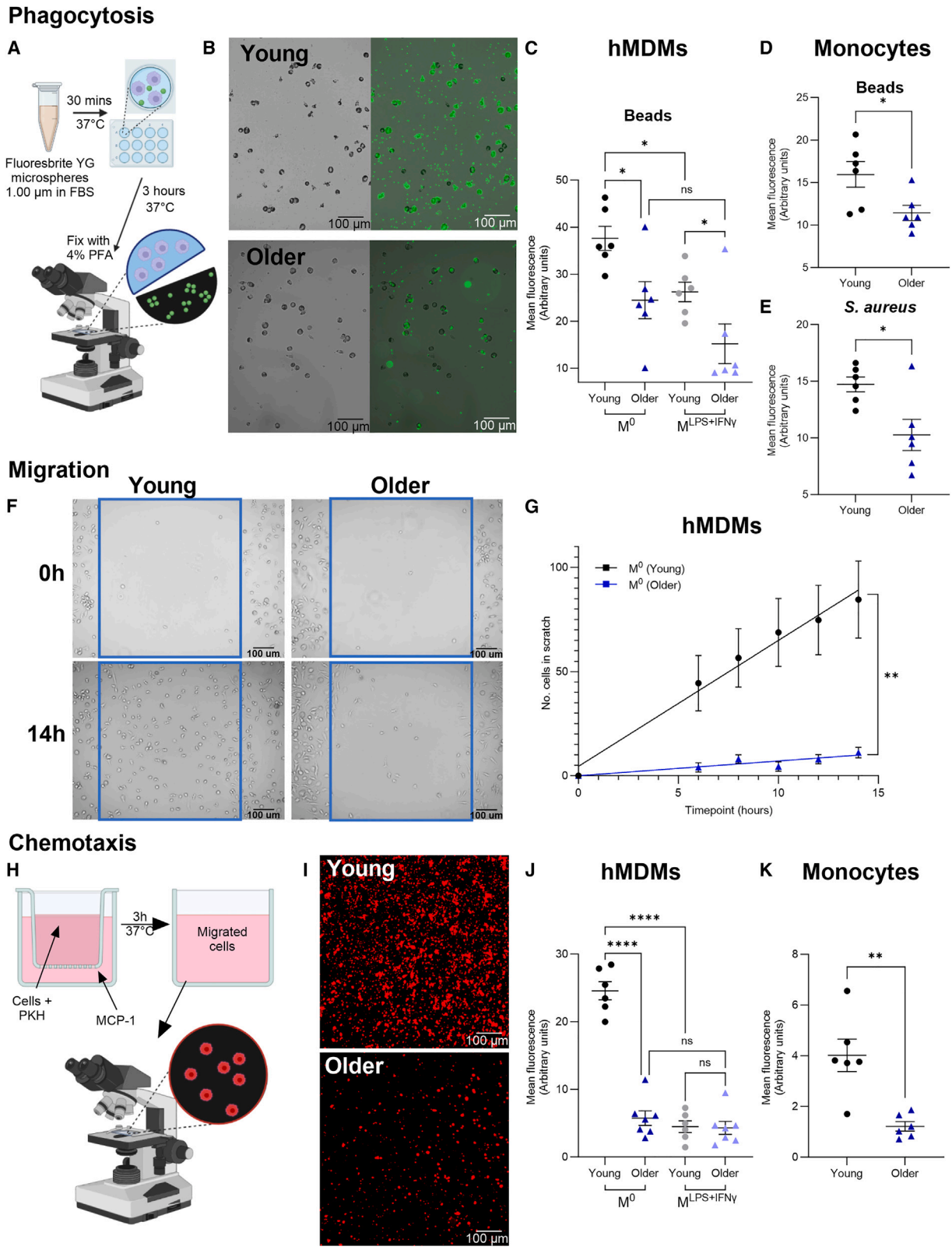

(legend on next page)

We further assessed monocyte chemoattractant protein 1 (MCP-1)-directed chemotactic migration (Figure 1H) and found that chemotaxis was reduced in both freshly isolated monocytes and M^0 MDMs with age. After 3 h, chemotaxis of M^0 MDMs was 77% lower in the older subjects compared with the M^0 MDMs from the younger group (Figures 1I and 1J). Similarly, in monocytes chemotaxis was 70% lower in the older subjects compared with the monocytes from the younger group (Figure 1K). As we observed above with migration, chemotaxis of the $M^{LPS+IFN\gamma}$ MDMs was significantly lower compared to the M^0 MDM population, and there was no difference between the two age groups (Figure 1J).

Overall, these results show a reduction in monocyte and M^0 MDM function with age.

Six transcription factors are associated with age-related transcriptomic alterations in murine alveolar macrophages

Having established a clear phenotypic difference in aged human M^0 MDMs (Figure 1), we set out to uncover the transcriptional networks that may drive these changes, with a focus on those that may be conserved across human and murine cells, an important *in vivo* mammalian model of aging. First, we analyzed a published microarray dataset of alveolar macrophages isolated from young (2–4 months) and old (22–24 months) C57BL/6J mice,[14] hypothesizing that TFs with many target genes differentially expressed with age would likely be governing the age-related changes seen in macrophage function. Although alveolar macrophages are tissue-resident cells with little monocyte infiltration during homeostasis, they primarily function in immune surveillance, making this dataset relevant to our work.[23,27]

Differentially expressed genes (DEGs) with age included 213 upregulated genes (log(fold change) [logFC] > 1.5, false discovery rate [FDR] < 0.05) and 122 downregulated genes (logFC < −1.5, FDR < 0.05; Figure S2 and Data S1). Enrichment analysis of these genes using the "ENCODE_and_ChEA_Consensus_TFs_from_ChIP-X" library in Enrichr was performed to identify the TFs responsible for differentially expressed transcripts (Figures 2A. 2B, and S2). While five TFs showed weak associations with upregulated genes (none of which reaching statistical significance, Figure 2A), six TFs (*Myc*, *Elf1*, *Foxm1*, *Nfyb*, *Usf1*, and *Srf*) were significantly associated with the downregulated gene group ($p < 0.05$) (Figure 2B). Assessment of expression of these TFs themselves between the young and aged alveolar macrophages (with focus on the TFs differentially expressed in the same direction as their target genes), showed that *Myc*, *Foxm1*, *Nfyb*, *Usf1*, and *Srf* were significantly downregulated and *Nfic* was upregulated with age, making them the most likely regulators to be driving age-related differential gene expression (Figures 2C–2E). In line with this, we found 29.3%–54.2% of the putative target genes of these TFs that are expressed in macrophages to be dysregulated with age (Figure 2F).

MYC and *USF1* are downregulated with age in human and murine macrophages, and their allelic variants are associated with monocyte percentage in human blood

To validate the six identified TFs as potential regulators of the observed aging human macrophage phenotype, we next compared mouse BMDMs isolated from young (2–4 months) and aged (22–24 months) C57BL/6J mice and MDMs from our human cohort (Figures 3A and 3B).

MYC and *USF1* showed consistent downregulation with age in both murine BMDMs and human MDMs, occurring in M^0 cells for *MYC* (while the inflammatory $M^{LPS+IFN\gamma}$ phenotype had a complete lack of expression) and in both M^0 and $M^{LPS+IFN\gamma}$ for *USF1*. These two TFs were therefore analyzed further to mechanistically assess their contribution to the aging macrophage phenotypes. Although some consistency was seen in the other assessed TFs compared to the previously analyzed murine alveolar macrophage data, lack of consistency across all assessed murine and human macrophage types meant that these were not taken forward.

Publicly available transcriptomic data suitable for the analysis of age-related changes in human macrophages is very limited. However, the Cardiogenics Consortium transcriptomic study dataset includes monocyte and MDM expression profiles and genotype information from 596 human donors of varying ages (42–65 years).[28–30] MDMs in this dataset have been cultured in a way consistent with those in the present study[28–30] so that we can consider them equivalent to our M^0 MDMs. To identify allelic variants of *MYC* and *USF1* associated with RNA levels for these TFs, we analyzed top and bottom age quartiles of this

Figure 1. Human MDM phagocytosis and chemotaxis are reduced with age

(A) Schematic diagram of phagocytosis assay design.
(B) Representative images of MDM uptake of fluorescent beads. Scale bar, 100 μm.
(C) Bead uptake expressed as mean fluorescence intensity for MDMs from young and older subjects after 3 h of incubation.
(D) Bead uptake expressed as mean fluorescence intensity for monocytes from young and older subjects after 3 h of incubation.
(E) *Staphylococcus aureus* uptake expressed as mean fluorescence intensity for monocytes from young and older subjects after 3 h of incubation.
(F) Representative images of MDMs returning to the scratch after 14 h of incubation. Scale bar, 100 μm.
(G) Number of MDMs returning to the scratch from young and older subjects over 14 h. Data are presented as mean ± SEM with each data point representing the mean of six donors, each done in triplicate.
(H) Schematic diagram of migration assay design.
(I) Representative images of PKH26-stained MDMs that migrated through the transwell. Scale bar, 100 μm.
(J) Migrated MDMs measured as mean fluorescence intensity from young and older subjects after 3 h of incubation.
(K) Migrated monocytes measured as mean fluorescence intensity from young and older subjects after 3 h of incubation.
In (C–E), (J), and (K), data are presented as mean ± SEM with each data point representing the mean of triplicate experiments done per donor for each condition. In (C–E), (G), (J), and (K), MDMs were differentiated from young (22–25 years, $N = 6$) and older (54–71 years, $N = 6$) healthy human donors. M^0, cells left unstimulated; $M^{LPS+IFN\gamma}$, cells stimulated with LPS and IFN-γ for 24 h. Two-way ANOVA with Tukey's multiple comparison, $^*p < 0.05$, $^{**}p < 0.01$, $^{****}p < 0.0001$. ns, not significant.

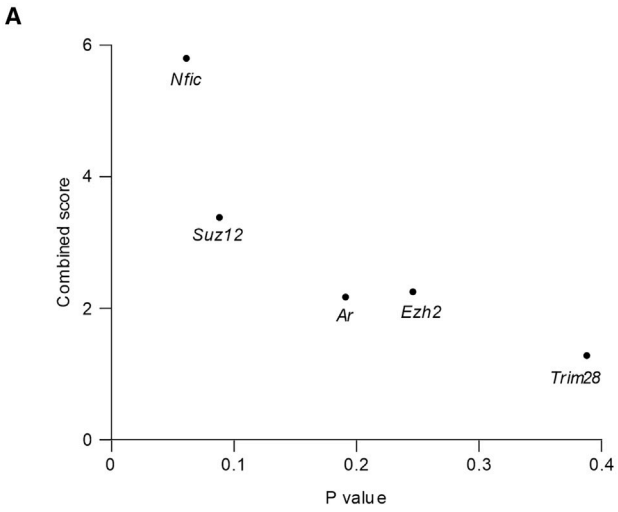

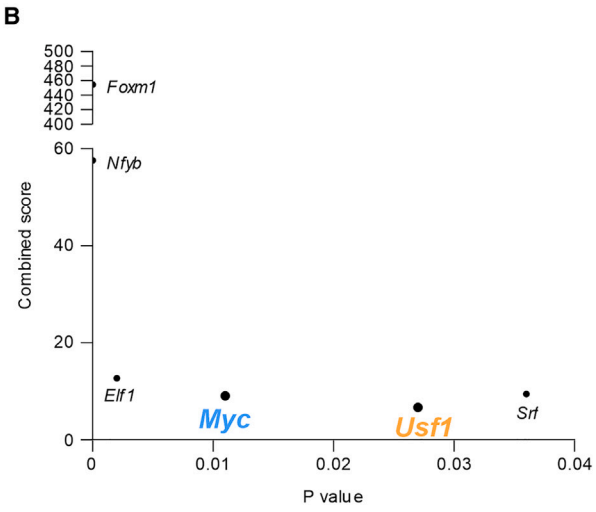

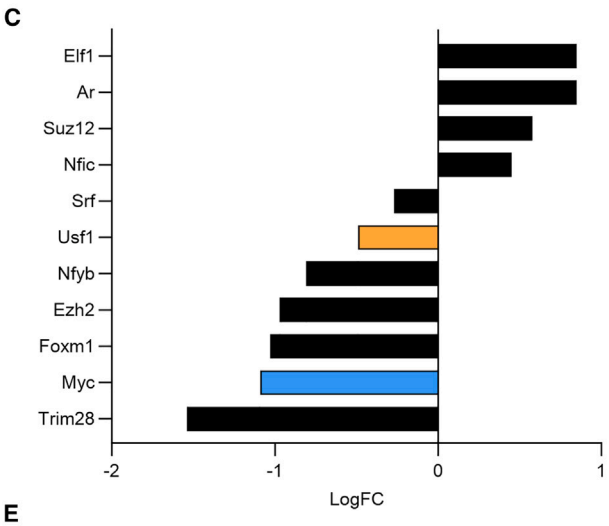

D

TF of interest	Direction of TF with age	Direction of target genes with age	P value
Foxm1	↓	↓	**$3x10^{-10}$**
Nfyb	↓	↓	**$7x10^{-9}$**
Myc	↓	↓	**0.01**
Usf1	↓	↓	**0.03**
Srf	↓	↓	**0.04**
Nfic	↑	↑	**0.06**
Elf1	↓	↑	**0.002**
Suz12	↑	↑	0.08
Ar	↑	↑	0.19
Trim28	↑	↓	0.39
Ezh2	↑	↓	0.25

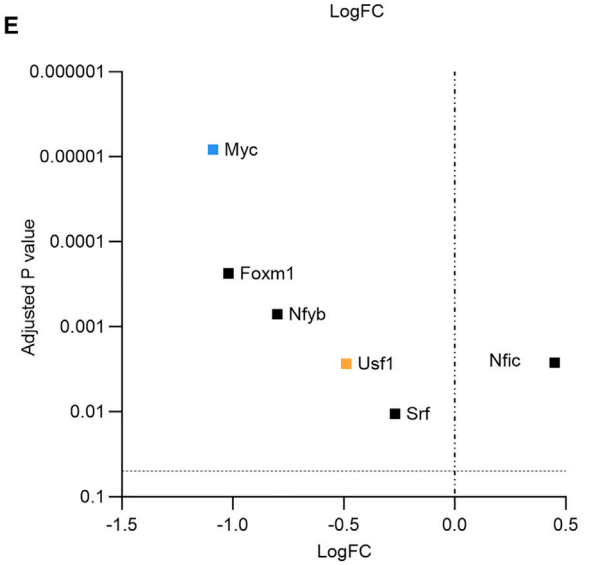

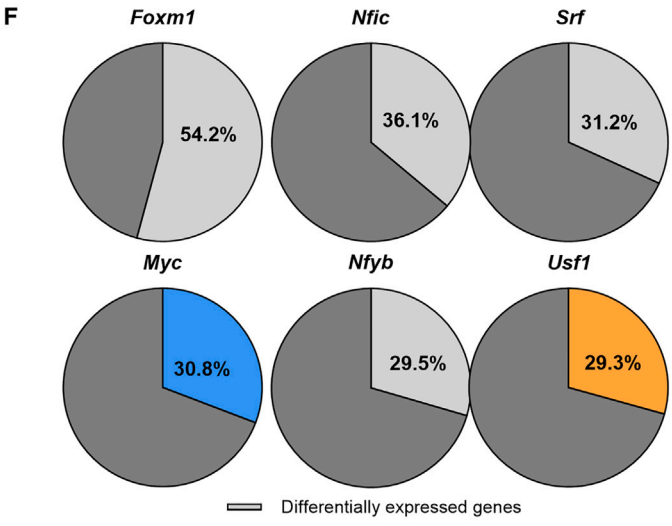

Figure 2. Transcription factors (TFs) associated with age-related DEGs in murine alveolar macrophages

(A) TFs associated with upregulated genes with age. Combined score measures a combination of *p* value and *Z* score to enable comparison of rankings. *p* value is calculated using Fisher's exact test.

(legend continued on next page)

dataset to identify expression quantitative trait loci (eQTLs). A total of 569 single-nucleotide polymorphisms (SNPs) were associated with *USF1*, and 36 SNPs were associated with *MYC* in monocytes (FDR < 0.05). A further 491 and 1 SNPs were associated with *USF1* and *MYC* in M^0 MDMs, respectively (Data S2). All of these were *cis*-eQTLs and for *USF1* represented three discrete association signals (Figure 3C). Exploration of other published datasets within Phenoscanner revealed a further seven signals (Table S2). Sentinels for all ten *USF1* associations were assessed for association with human traits and disease in genome-wide association study catalogs and databases, including Phenoscanner and Open Target. The most notable genome-wide associations were found to be with blood cell traits, including blood monocyte percentage (Table S3). While data on age-related changes in blood monocyte counts are sparse and there is currently no consensus on whether this is altered in aged individuals, it is widely accepted that the ratio of classical ($CD14^+CD16^-$) vs. non-classical ($CD14^{dim}CD16^+$) monocytes is altered, with the non-classical monocyte subset expanding during aging. Therefore, we assessed *MYC* and *USF1* expression between classical and non-classical monocyte subsets through a combined analysis of four published datasets, equating to 15 individual samples per monocyte subset.[31–34] RNA levels of *MYC* and *USF1* were normalized to the expression of *PUM1* in each dataset, a housekeeping gene found to be consistent across our polarized and older cell populations, so that data from the individual datasets could be pooled and analyzed together. We found *MYC* expression to be downregulated in $CD14^{dim}CD16^+$ monocytes compared with the $CD14^+CD16^-$ population (Figures 3D and 3E), suggesting that the age-related reduction in *MYC* RNA levels could, at least in part, be due to the expansion of the low *MYC*-expressing nonclassical monocyte subset. We further assessed the expression of *MYC* and *USF1* with age in freshly isolated human monocytes, whereby we found that *MYC* but not *USF1* was downregulated in those isolated from older individuals (Figure 3F), in keeping with the transcriptomic analysis. Further, we tested whether expression of *MYC* and *USF1* target genes were altered with age in the Cardiogenic Consortium dataset by comparing top and bottom age quartiles, comprising 201 donors in each age group. Among the DEGs with age (FDR < 0.05) in these monocytes and M^0 MDMs, more than 20% were putative *MYC* and *USF1* targets (Figure 3G and Data S2). Those with logFC > 0.1 are shown in Figure 3H. The significance of *MYC* target gene expression in these macrophages was further assessed by gene set enrichment analysis (GSEA) of hallmarks, where MYC targets v1 and v2 were significantly enriched (FDR < 2.2e−16) between the top and bottom quartiles of *MYC* expression (Data S2).

Putative MYC and USF1 targets were also assessed in other published datasets related to this research, including GEO: GSE155992, where MYC itself was downregulated with age (adjusted $p = 0.0034$) alongside 16% of MYC targets and 7% of USF1 targets being dysregulated. Additionally, GEO: GSE111382 and GSE100905 were found to have more than 10% of DEGs with age (FDR < 0.05) in MYC targets and 5% in USF1 targets (Data S4).

Loss of *MYC* or *USF1* in young human MDMs is sufficient to recapitulate an aging macrophage phenotype

Since older human macrophages displayed reduced function, and as both *MYC* and *USF1* were consistently downregulated with age across murine and human macrophage populations, we next investigated whether *MYC* or *USF1* expression levels are causatively linked to macrophage function. We tested this by a transient knockdown of *MYC* or *USF1* in MDMs from young human subjects and explored whether this could model the aging macrophage phenotype.

Both *MYC* and *USF1* were well expressed in young M^0 populations and downregulated with age. *USF1* was also expressed in the $M^{LPS+IFN\gamma}$ phenotype and was also downregulated with age (Figure 3B). Expression of *MYC* and *USF1* showed no consistency in age-related dysregulation in interleukin-4-stimulated (M^{IL-4}) macrophages, tested because of *MYC* expression being well documented in this macrophage phenotype (Figure S3). To test whether loss of *MYC* or *USF1* is sufficient to cause an old macrophage phenotype, we used small interfering RNA (siRNA) gene silencing. The efficiency of *MYC* gene silencing was 97% (86.4%–99.9%), and the efficiency of *USF1* gene silencing was 95% (81.3%–99.9%) in M^0 and 83% (46.9%–99.4%) in $M^{LPS+IFN\gamma}$ MDMs (Figure 4A); downregulation of MYC protein was assessed by western blotting (Figure S4). Consistent with the aged MDM phenotype, phagocytosis was reduced in both si*MYC* M^0 and si*USF1* M^0 compared with control M^0. There was no further reduction in phagocytosis in si*USF1* $M^{LPS+IFN\gamma}$ cells compared with $M^{LPS+IFN\gamma}$ controls (Figure 4B). Similarly, migration and MCP-1 chemotaxis were reduced in both si*MYC* M^0 and si*USF1* M^0 compared with M^0 control (Figures 4C and 4D).

Loss of *MYC* or *USF1* in young human MDMs reproduces the transcriptomic signature of older macrophages

To further evidence the causative role of *MYC* and *USF1* loss in the older macrophage phenotypes we had identified, we compared the transcriptomic signature of gene-silenced vs. unmodified MDMs from the younger subjects (Figure 5). Principal component analysis (PCA) of transcripts that were dysregulated

(B) TFs associated with downregulated genes with age. Combined score measures a combination of *p* value and *Z* score to enable comparison of rankings. *p* value is calculated using Fisher's exact test.
(C) Direction and magnitude of differential expression of TFs associated with target gene list in aged vs. young murine alveolar macrophages.
(D) Ranking of TFs, differentially expressed with age: differentially expressed in the same direction as the target gene list, significant association with target gene list ($p < 0.05$).
(E) Fold change of TF expression and *p* values adjusted for multiple-testing correction. Adjusted *p* value is calculated using Benjamini-Hochberg false discovery rate (FDR) < 0.05.
(F) Percentage of TF target genes expressed in macrophages that are dysregulated with age. *Foxm1*, 45 differentially expressed/of 83 targets; *Nfic*, 73/202; *Srf*, 82/263; *Myc*, 412/1,336; *Nfyb*, 886/3,004; *Usf1*, 352/1,200. Differentially expressed genes with age (logFC > 1.5) were identified in GEO: GSE84901 microarray dataset comparing alveolar macrophages from young (2–4 months, $N = 6$) and aged (22–24 months, $N = 6$) C57BL/6J mice.

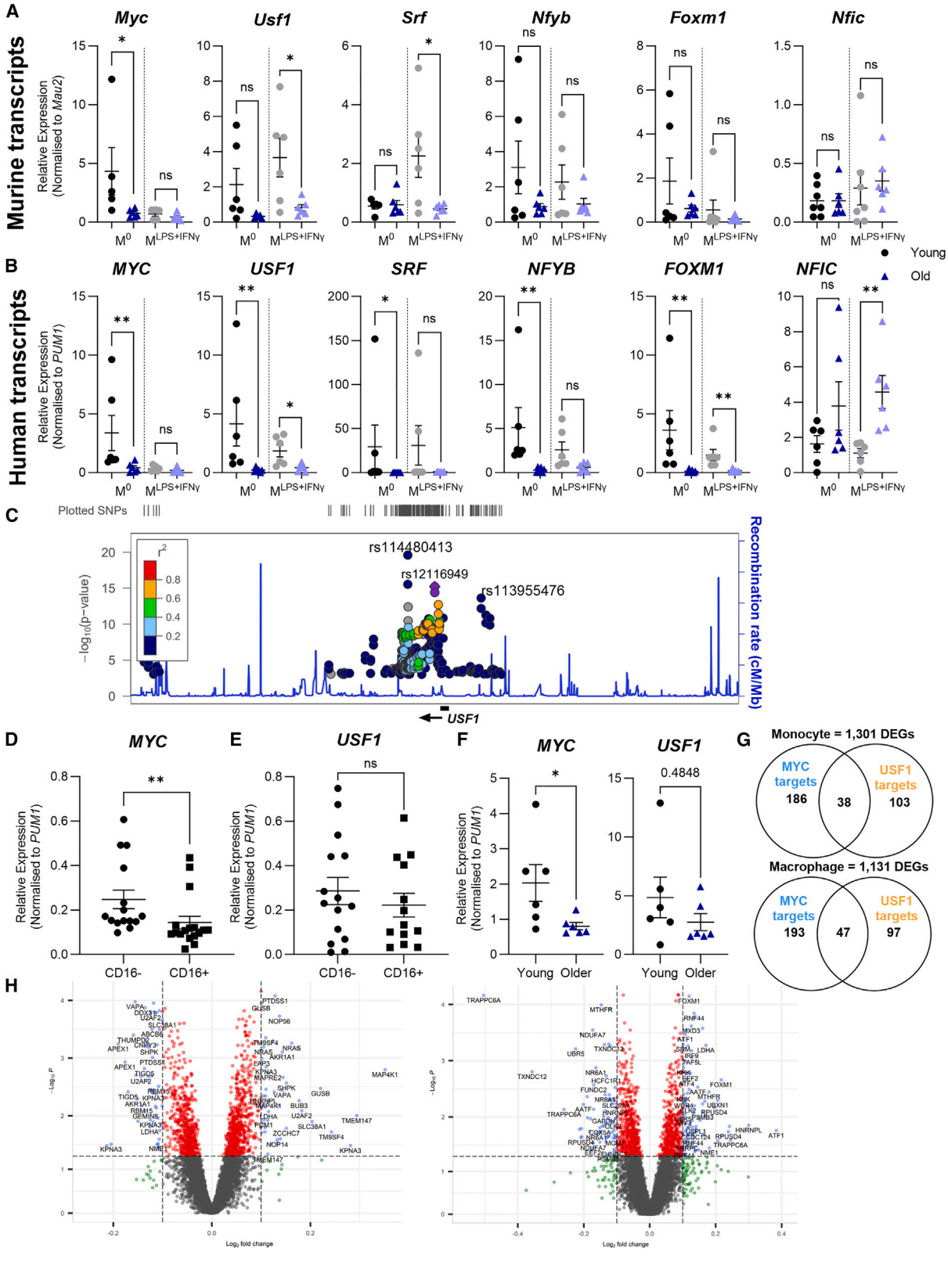

(legend on next page)

showed a significant clustering of the knockdown conditions, extending to 5,872 DEGs ($p < 0.05$) between si*MYC* M^0 and M^0 control (Figure 5A), 6,148 DEGs between si*USF1* M^0 and M^0 control (Figure 5B), and 6,350 DEGs between si*USF1* $M^{LPS+IFN\gamma}$ and $M^{LPS+IFN\gamma}$ control (Figure 5C and Data S3). An overall PCA of all samples also showed clustering of males and females (Figure 5).

Among the DEGs between si*MYC* M^0 and M^0 control (FDR < 0.05), associated hallmark gene sets[35] included MYC targets and mTORC1 (mammalian target of rapamycin complex-1) signaling (Data S3). Enriched biological processes included cell-cell adhesion and extracellular matrix (ECM) formation (Figure 5A). Between si*USF1* M^0 and M^0 control, cell-cell adhesion and development processes were enriched (Figure 5B). DEGs were also linked to hallmark gene sets including MYC targets and glycolysis (Data S3). DEGs between si*USF1* $M^{LPS+IFN\gamma}$ and $M^{LPS+IFN\gamma}$ control were linked to hallmark gene sets such as hypoxia and angiogenesis (Data S3). Enriched biological processes included cell-cell adhesion and ion transport (Figure 5C).

To complement the analysis of human macrophages, we returned to our mouse transcriptional network dataset comparing young and aged alveolar macrophages and performed GSEA on the DEGs, this time including all significant genes (FDR < 0.05).[14] Cell-cell adhesion and ECM components were also enriched biological processes. Hallmarks associated with DEGs included MYC targets and G_2M checkpoint (Data S1).

As many DEGs were associated with similar hallmarks and biological processes, we next assessed whether the same set of DEGs were also dysregulated in older human MDMs. DEGs were ranked by logFC, *p* value, and the number of times they appeared in different enriched gene sets (Figures 6A–6C). Genes with logFC > 1.3 and appearance in at least five enriched gene sets ($p < 0.05$) and that showed relevance to macrophage function through the literature search were then analyzed by RT-qPCR in human MDMs. Expression levels of 22 genes were assessed (Figure 6D), and nine of these had reproducible differential expression in older vs. young MDMs as was found between TF knockdown vs. control (Figures 6E, 6F, and S6). Finally, specific analysis of *CCR2* (the MCP-1 receptor) demonstrated reduced expression, providing a possible mechanism for dysregulation in MCP-1 chemotaxis[36] between si*MYC* M^0 and M^0 control and between old and young murine M^0 BMDMs (Figure S6).

Age and loss of *MYC* or *USF1* in young human MDMs alter cytoskeletal structure

Having established the sufficiency of *MYC* and *USF1* loss in recapitulating the old macrophage phenotype, we used the above analysis of biological processes (Figure 4) to predict further mechanistic factors in the aging macrophage phenotype. As we found genes associated with cell-cell adhesion, ECM components, and the cytoskeleton enriched in our analysis, we hypothesized that cytoskeletal and cell morphological changes would be altered in older macrophages and those with loss of *MYC* or *USF1*. It has previously been established that F-actin content is a strong determinant of a cells' ability to survey the local environment, move through the tissue, and produce the phagosome required for phagocytosis.[37–39] Additionally it is known that the circularity of the cell is strongly associated with motility, with a more elongated phenotype being preferential for this function.[40] We predicted that older macrophages and those with loss of *MYC* or *USF1* would exhibit a more spread, adhesive appearance and reduced capability for actin motility. To test our prediction we measured cell size, circularity, and F-actin (Figure 7) and found that older M^0 MDMs were larger in size, less circular, and had less F-actin content compared with young counterparts. Older $M^{LPS+IFN\gamma}$ MDMs were also more elongated than young counterparts. Comparing young MDMs, M^0s were smaller and had less F-actin content than $M^{LPS+IFN\gamma}$ MDMs. Finally, older M^0 MDMs were larger with less F-actin content than older $M^{LPS+IFN\gamma}$ MDMs (Figures 7B–7D). Similarly, compared with M^0 control, si*MYC* M^0 MDMs had increased size and elongation, while si*USF1* M^0 MDMs had increased elongation as well as reduced F-actin content. Compared with $M^{LPS+IFN\gamma}$ controls, si*USF1* $M^{LPS+IFN\gamma}$ MDMs had increased elongation (Figures 7E–7G).

Thus, having identified an old macrophage phenotype in human MDMs, we have uncovered *MYC/USF1* transcriptomic regulation of macrophage chemotaxis and phagocytosis, paired with cytoskeletal and receptor changes that can be recapitulated in young macrophages by reducing *MYC* or *USF1* RNA levels.

Figure 3. Transcription factor expression with age in murine bone marrow-derived macrophages and human MDMs and genetic associations

(A) Age-related changes in expression of TFs in BMDMs isolated from young (2–5 months, $N = 6$) and aged (22–24 months, $N = 6$) C57BL/6J mice. *Mau2* expression was used as a housekeeping control.

(B) Age-related changes in expression of TFs in MDMs isolated from young (22–25 years, $N = 6$) and older (54–71 years, $N = 6$) healthy human donors. *PUM1* expression was used as a housekeeping control. In (A) and (B), data are presented as mean ± SEM with each data point representing the mean of triplicate experiments done per donor. M^0, cells left unstimulated; $M^{LPS+IFN\gamma}$, cells stimulated with LPS and IFN-γ for 24 h. Mann-Whitney test, $^*p < 0.05$, $^{**}p < 0.01$.

(C) Manhattan plot of discrete signals of eQTLs associated with USF1 in Cardiogenic Consortium transcriptomic study monocytes ($N = 596$).

(D) Relative expression of *MYC* in monocyte subsets from published datasets.

(E) Relative expression of *USF1* in monocyte subsets from published datasets. In (D) and (E), *PUM1* expression was used as a control to normalize all samples. $N = 15$, Mann-Whitney test, $^{**}p < 0.01$.

(F) Relative expression of *MYC* and *USF1* in monocytes isolated from young ($N = 6$, 22–25 years) and older ($N = 6$, 54–71 years) human subjects. *PUM1* expression was used as a housekeeping control. Data are presented as mean ± SEM with each data point representing the mean of triplicate experiments done per donor. Mann-Whitney test, $^*p < 0.05$.

(G) Association between MYC and USF1 targets and DEGs with age in Cardiogenics Consortium transcriptomic study monocytes (left) and macrophages (right) ($N = 596$).

(H) Volcano plots of MYC and USF1 targets in DEGs with age in Cardiogenic Consortium transcriptomic study monocytes (left) and macrophages (right) ($N = 596$). Log_2FC thresholds are illustrative and not used for differential expression analysis of genes.

ns, not significant.

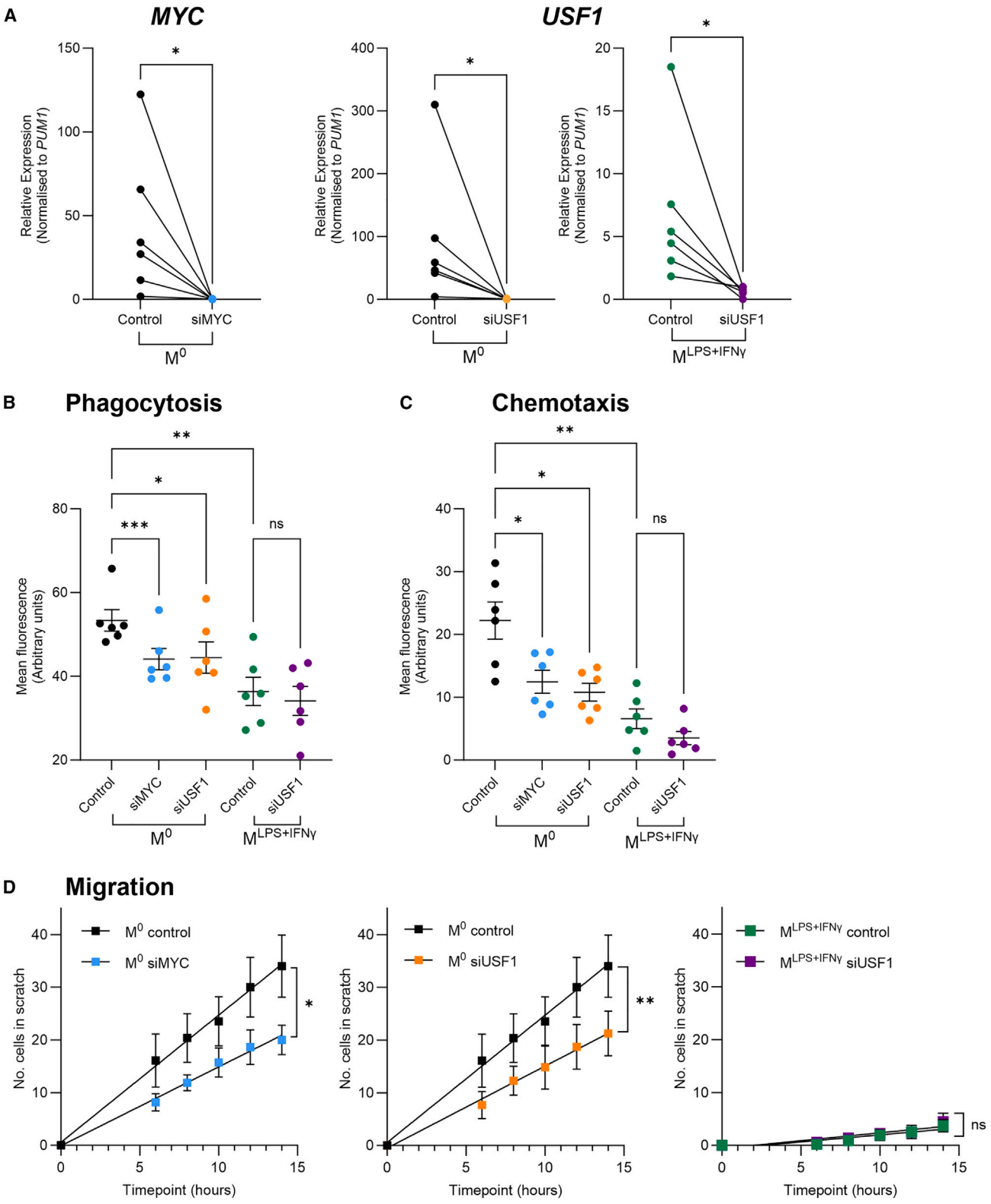

Figure 4. Loss of *MYC* or *USF1* in young human primary macrophages reduces phagocytosis and chemotaxis

(A) Relative expression of *MYC* or *USF1* in respective siRNA knockdowns in MDMs isolated from young donors. Each data point represents the mean of triplicate experiments done per donor ($N = 6$). *PUM1* expression was used as a housekeeping control. Mann-Whitney test, $^{*}p < 0.05$.

(legend continued on next page)

DISCUSSION

In this study, we revealed a key role of *MYC* and *USF1* transcriptional networks in age-related macrophage functional decline. We found that aging led to a decrease in macrophage phagocytosis, migration, and chemotaxis, as well as increased cell size and elongation. Loss of either *MYC* or *USF1* in young macrophages resulted in comparable functional decline and morphology, modeling the changes seen with age. We identified *MYC* and *USF1* transcripts to be downregulated with age in both murine and human macrophage populations, alongside dysregulation of transcriptional targets that may be driving age-dependent changes in function and morphology in older human macrophages.

To date, most of our understanding of macrophage aging has been reported from mouse tissue populations, and there is a gap in functional and mechanistic understanding in human cells. Age-related changes are less well defined in MDMs, which play a key role in age-related diseases including atherosclerosis, diabetes, and fibrosis. We therefore assessed macrophage dysfunction with age in human MDMs, showing both phagocytosis and chemotaxis to be reduced with age. It is worth noting that monocyte counts between the young and older cohorts were comparable and not likely influencing these changes (10.27 ± 3.13 million vs. 9.36 ± 2.9 million cells, respectively isolated from 80 mL of blood). No real consensus has been drawn on changes in macrophage number with age, with large tissue- and stimulus-specific variation, although it has been suggested that pro-inflammatory populations increase with age.[6] Interestingly, LPS and IFN-γ activation caused a slight but significant reduction in phagocytosis compared with M^0 in both the young and older cohorts, contradicting published literature suggesting phagocytosis to be a principally inflammatory immune response.[41] Peritoneal macrophages that had been polarized with M1-like or M2-like stimuli showed comparable phagocytic activity with age following M2 polarization, but reduced phagocytosis with age in M1-like macrophages, similar to our findings.[42] Fix et al. also found an impairment in phagocytosis with age in pro-inflammatory BMDMs.[16] In contrast to our findings in human MDMs, IFN/LPS stimulation has been found to increase phagocytosis in both young and old BMDMs.[17] In our findings, LPS and IFN-γ stimulation of M^0 MDMs from young human subjects led to a complete loss of chemotactic ability, while chemotaxis in the M^0 MDMs from older subjects was also comparable to that seen in the young $M^{LPS+IFN\gamma}$ MDMs, potentially demonstrating a chronically activated phenotype in the older M^0 MDMs and fitting with our current understanding of inflammaging.[3,5] Both phagocytosis and chemotaxis functions have been positively correlated with improved murine lifespan.[43,44] Chemotaxis accounted for 50% of variance in lifespan, and chemotaxis and phagocytosis together were found to predict almost 70% of final achieved lifespan, again with lower function being associated with shorter lifespan.[45]

Systematic gene enrichment analysis of mouse alveolar macrophage transcripts identified that specific TFs *Myc*, *Foxm1*, *Nfyb*, *Usf1*, and *Srf* were downregulated and *Nfic* was upregulated with age. Consistent with this, we identified downregulated *Myc* and *Usf1* in old mouse BMDMs and in human MDMs from older donors, which led us to assess whether knockdown of *MYC* and *USF1* in young human MDMs could recapitulate an aging phenotype. Loss of *MYC* and *USF1* significantly reduced both phagocytosis and chemotaxis in young macrophages. MYC is well established to play a key role in regulating the cell cycle as well as cell metabolism, tissue remodeling, and pro- and anti-inflammatory cytokine production.[46,47] It is known to be a central marker for alternative macrophage activation, controlling expression of nearly half of the genes associated with macrophage alternative activation, partly through upregulation of STAT6 (signal transducer and activator of transcription-6) and PPARγ (peroxisome proliferator-activated receptor-γ) signaling.[48,49] MYC is also implicated in the growth and progression of many cancer types,[50] shown to be the most common abnormality in malignant tumors.[51] Takahashi and Yamanaka discovered that the introduction of *MYC* alongside three other TFs can reprogram differentiated cells back to a stem cell-like state[52]; short-term cyclical expression of these factors can ameliorate hallmarks of aging and prolong lifespan,[53] the first indication of *MYC*'s potential involvement in the aging of cells. *MYC* has since been implicated in aging, with its expression having a key role in proper mitochondrial function[54,55] and in regulation of double-stranded DNA breaks, extensively reviewed elsewhere.[56] Mitochondrial dysfunction and genomic instability are two of the hallmarks of aging.[57] The downregulation in Foxm1 with age that we found in the mouse alveolar macrophages and BMDMs is also intriguing, given the association between this TF and senescence. Foxm1 has previously been shown to decline with age in human dermal fibroblasts,[58] potentially as a result of activation of the p53-p21-DREAM pathway that prevents expression of early cell-cycle genes.[59] This could therefore be indicative of a more senescent phenotype within these macrophage populations.

USF1 has been shown to drive dysregulated cardiometabolic health[60] and cancers such as adenocarcinoma, where *USF1* expression may activate the *MYC* pathway,[61] highlighting established links between these TFs. *USF1* responds to dietary components such as glucose, and recognizes the E-box CACGTG motif promoter region of target genes, many of which are involved in lipid metabolism.[62] Many studied polymorphisms in

(B) Bead uptake expressed as mean fluorescence intensity from young human MDMs with loss of *MYC* or *USF1* after 3 h of incubation.
(C) Migrated MDMs measured as mean fluorescence intensity from young human MDMs with loss of *MYC* or *USF1* after 3 h of incubation. In (B) and (C), data are presented as mean ± SEM with each data point representing the mean of triplicate experiments done per donor. $N = 6$, repeated-measures one-way ANOVA with Tukey's multiple comparison, $^*p < 0.05$, $^{**}p < 0.01$, $^{***}p < 0.001$.
(D) Number of MDMs returning to the scratch from young human MDMs with loss of *MYC* or *USF1* over 14 h. Data are presented as mean ± SEM with each data point representing the mean of six donors, each done in triplicate. $N = 6$, two-way ANOVA with Tukey's multiple comparison, $^*p < 0.05$, $^{**}p < 0.01$.
Control, non-targeting siRNA control; siMYC, MYC-targeting siRNA; siUSF1, USF1-targeting siRNA; M^0, cells left unstimulated; $M^{LPS+IFN\gamma}$. cells stimulated with LPS and IFN-γ stimulated for 24 h. ns, not significant.

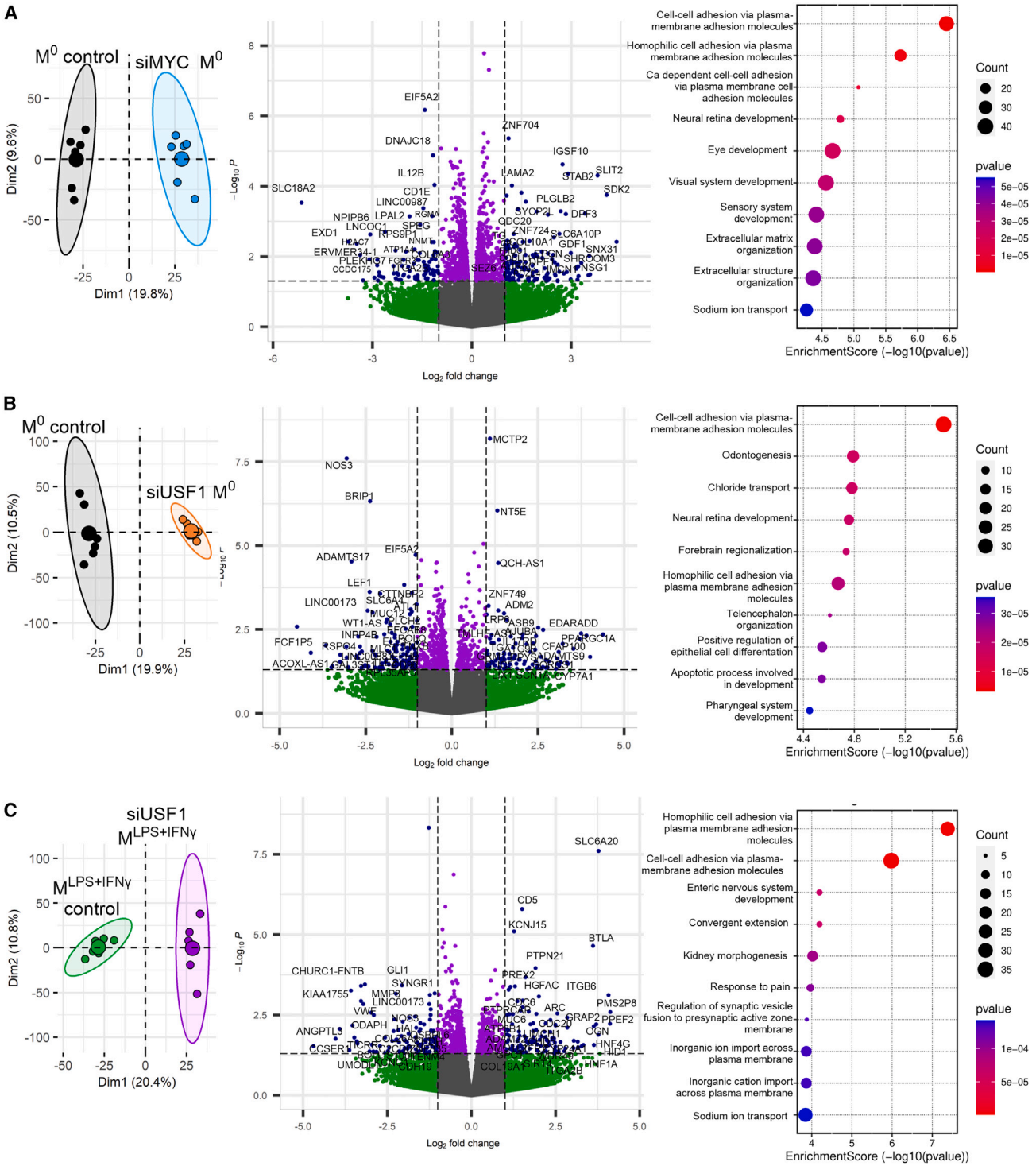

Figure 5. Loss of *MYC* or *USF1* produces changes in transcriptional signature associated with macrophage function

Principal component analysis of transcripts dysregulated in different conditions showing the first two dimensions (left), volcano plot showing DEGs (logFC > 1, $p < 0.05$) with logFC thresholding added for illustrative purposes only and not used for differential expression analysis of genes (center), and dot plot showing associated enriched biological processes with count indicating the number of genes dysregulated in the pathway (right) in young MDMs for si*MYC* M^0 vs. M^0 control (A), si*USF1* M^0 vs. M^0 control (B), and si*USF1* $M^{LPS+IFN\gamma}$ vs. $M^{LPS+IFN\gamma}$ control (C).

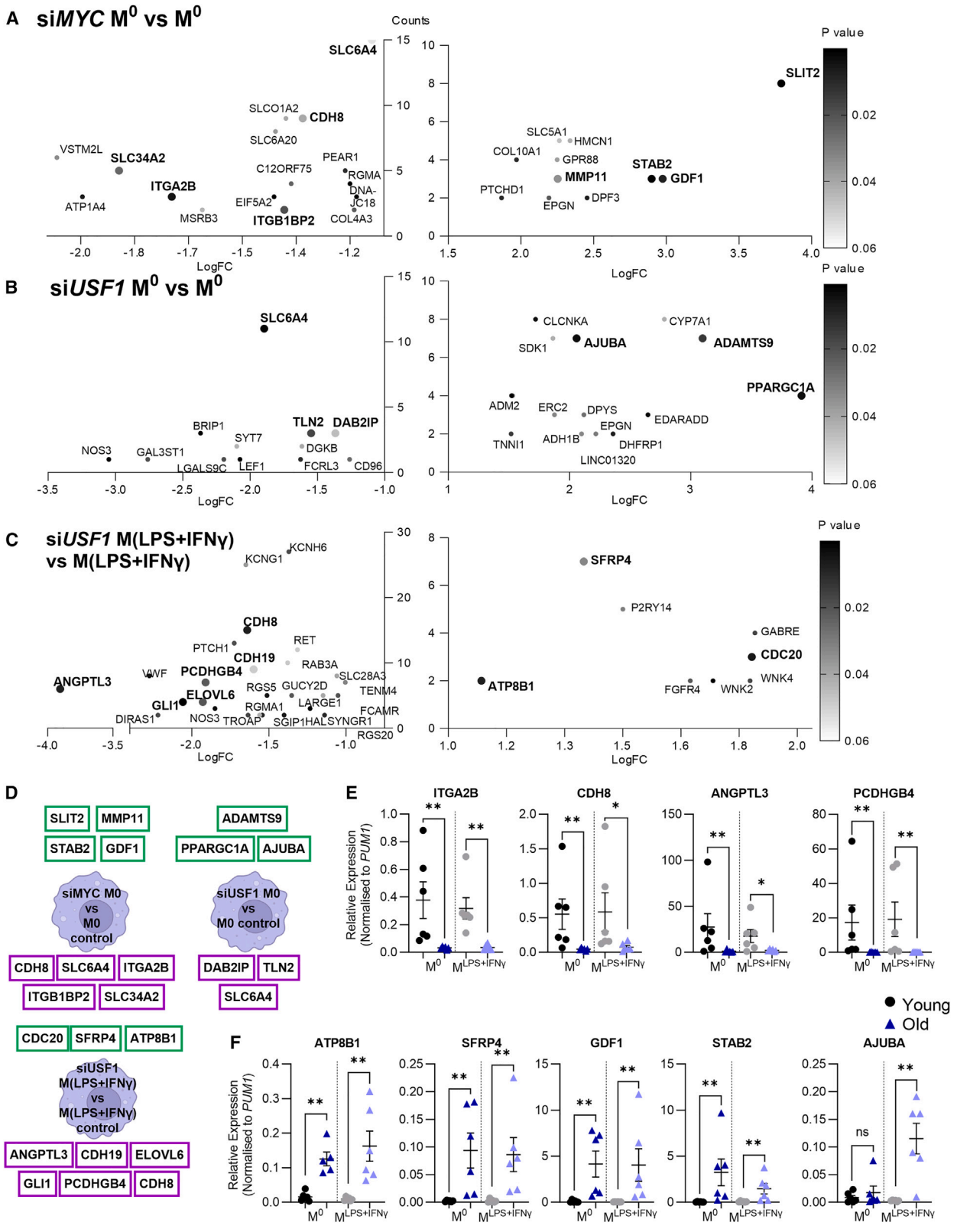

(legend on next page)

USF1 SNPs have strong associations with plasma lipid levels, apolipoprotein E gene expression, and familial hyperlipidemia.[63,64] The rs3737787 and rs2073658 genetic variants of *USF1* have significant associations with familial hyperlipidemia, a risk factor for premature cardiovascular disease affecting pro-inflammatory cytokine secretion and serum lipid levels.[65] Further, *USF1* SNPs such as rs10908821 have an age-related association with brain lesion development in Alzheimer's disease.[66] This study has identified that *USF1* polymorphisms in macrophages and monocyte transcripts are associated with decreased monocyte percentage, a known age-related change. Monocyte numbers are known to become dysregulated with age, with non-classical pro-inflammatory monocytes becoming the central population of the aged immune system.[67,68] Our analysis showed that *MYC* is downregulated in the non-classical compared with classical monocytes, which fits with these existing data. There are clear genetic associations linked to *USF1* and age-related disease. Further, the presence of many *MYC* and *USF1* downstream targets in the DEGs of macrophages and monocytes from the Cardiogenic Consortium transcriptomic study cannot be understated. Assessing a single gene, such as the TF itself, is an unreliable estimation of TF binding activity, especially when effect size is small, such as that of the relatively limited age range analyzed in this dataset.[25,69] By instead using TF targets, a more reliable estimation of TF activity is achieved. This, therefore, further adds to our hypothesis that *MYC* and *USF1* are driving transcriptional and, therefore, functional changes with age.

We found that human MDMs show a profound reduction in phagocytosis, migration, and chemotaxis with age and investigated the mechanistic basis for these functional changes by assessing cytoskeletal rearrangement required for coordinated phagocytosis and migration.[70] Macrophage cytoskeleton is composed of cortical filamentous actin (F-actin), found in large ruffles in resting macrophages that survey the local environment and become phagosomes.[71] We found reduced F-actin content in older MDMs and with loss of *USF1*, suggesting a decline in cytoskeletal function in age, regulated by *USF1*, which may be contributing to reduced phagocytic capacity. Further, macrophage elongation has been shown to be essential for motility.[72] This correlates with our finding that the young M^0 MDMs are more motile and elongated than the $M^{LPS+IFN\gamma}$ MDMs; however, both phenotypes of the older MDMs had increased elongation, making this an unlikely mechanism for the reduced motility observed. Similar to our findings that older MDMs were larger than younger counterparts, older human cochlea macrophages were found to have a reduced number of processes projecting and increased cytoplasmic volume around the nucleus compared with young counterparts.[73] Interestingly, aging-impaired actin function linked to Rac1 has been shown to reduce alveolar macrophage phagocytosis of bacteria.[15]

Microglia have also been found to have altered morphology and functions with age. Similar to our findings, aged microglia have larger cell bodies[74] and are less mobile and phagocytic than young microglial cells.[75,76] Aged microglia have been associated with an increased state of inflammation[77] and display an amoeboid-like structure that was not seen in young microglia that may be linked to their reduced function.[78]

Migration requires complex adhesion interactions with other cells and the underlying ECM, a biological process that we found to be enriched by TF knockdown in human MDMs and with age in murine alveolar macrophages, with integrins and cadherins making up key dysregulated genes in human MDM aging. Adherence has previously been assessed in mice with consistent findings. Peritoneal macrophages show an increase in adherence capacity with age to smooth plastic meant to resemble tissue,[20] fibronectin, and type 1 collagen.[79] Cell adhesion pathways were also disturbed with aging in transcriptomic analysis of microglia.[80] This was comparable to the analysis performed here with six shared dysregulated genes associated with cell adhesion (PCDHGA2, AJUBA, CDH2, CXADR, TENM4, and CLDN1).

Transcriptional targets of *MYC* and *USF1* that we found to be dysregulated with age suggest several further mechanisms for the aging macrophage phenotype. *ANGPTL3* regulates lipoprotein lipase activity shown to be involved in age-related diseases such as atherosclerosis, already identified as a potential druggable target to treat this disease.[81] Targeting *STAB2* ameliorates atherosclerosis by dampening inflammation.[82] *ATP8B1* is associated with macrophage efferocytosis and resolution of inflammation and may be a potential therapeutic target in chronic pancreatitis.[83] *SFRP4* is involved in Wnt signaling and has been implicated in skin aging through promoting senescence-associated secretory phenotype (SASP), while its knockdown suppressed SASP.[84] *SFRP4* is upregulated with age, correlating with our data and suggesting a role in macrophage chronic inflammation and aging. Finally, *GDF1* is associated with cellular migration through Smad signaling in macrophages.[85] We also considered loss of the MCP-1 receptor, C-C motif chemokine receptor 2 (CCR2), as a possible mechanism for reduced migration. It has been shown that changes in CCL2-CCR2 interaction may affect macrophage polarization toward M1, with lower CCR2 expression contributing to increased M1 polarization and higher pro-inflammatory cytokine release.[36] Although *CCR2* mRNA levels were downregulated with loss of *MYC* in

Figure 6. Age-related changes in gene expression are mimicked by loss of *MYC* or *USF1* in young MDMs

(A–C) Leading-edge analysis of genes differentially expressed in si*MYC* M^0 vs. M^0 control (A), si*USF1* M^0 vs. M^0 control (B), or si*USF1* $M^{LPS+IFN\gamma}$ vs. $M^{LPS+IFN\gamma}$ control (C), showing genes downregulated (left) and genes upregulated (right) plotted as number of enriched gene sets that the gene is associated with (y axis) against the fold change of the gene (x axis). Color gradient of the dot corresponds to *p* value, and dots of larger size were taken forward due to scoring highly in each field and association with macrophage function in the literature search.

(D) Selected genes from each comparison taken forward for assessment in young and older human MDMs. Green, upregulated genes; purple, downregulated genes.

(E and F) Age-related changes in expression of selected genes in MDMs isolated from young (22–25 years, $N = 6$) and older (54–71 years, $N = 6$) healthy human donors that corresponded to genes upregulated (E) or downregulated (F) in TF knockdown RNA-sequencing analysis. *PUM1* expression was used as an internal control.

M^0, cells left unstimulated; $M^{LPS+IFN\gamma}$, cells stimulated with LPS and IFN-γ for 24 h. Mann-Whitney test, $^*p < 0.05$, $^{**}p < 0.01$.

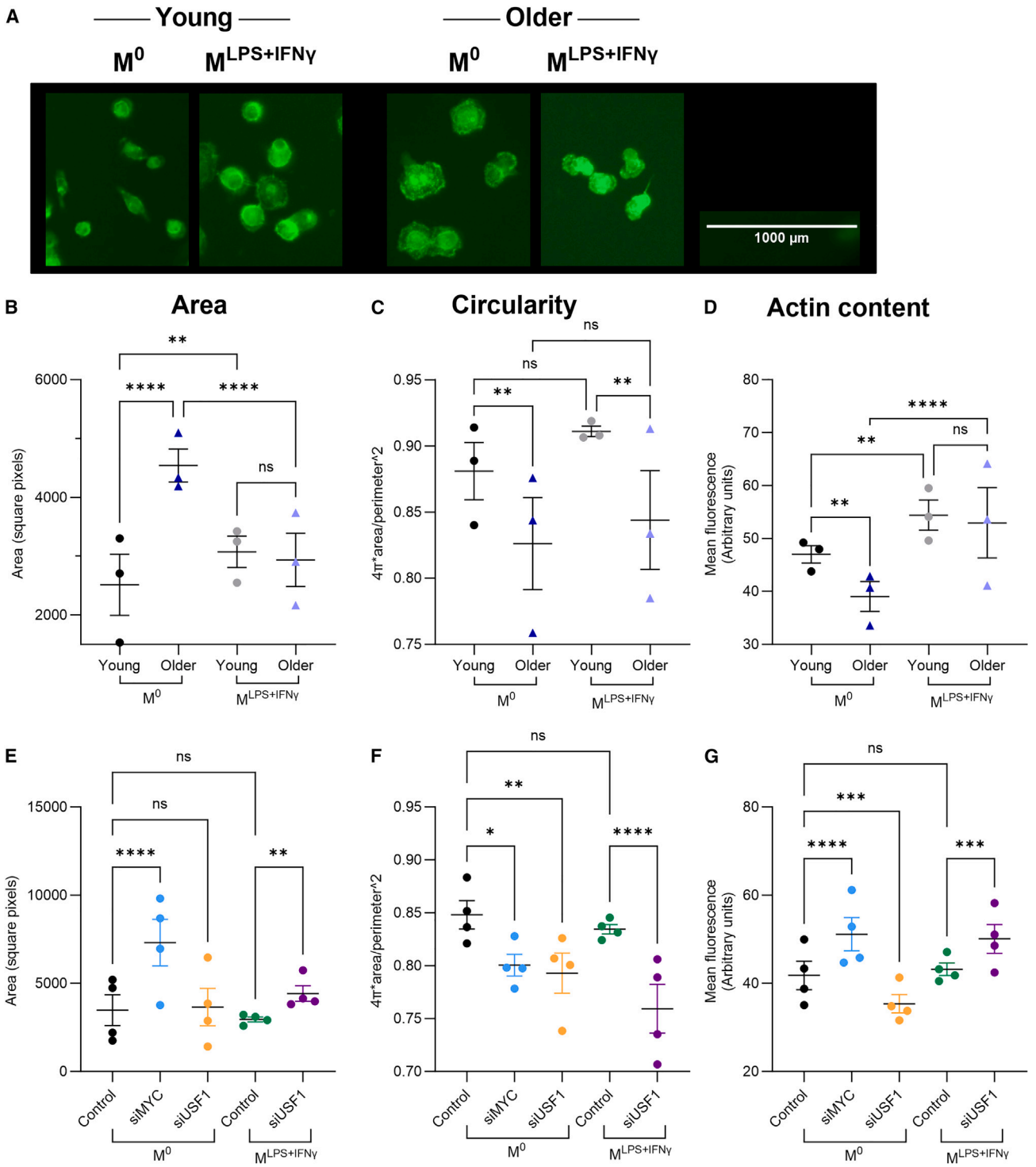

Figure 7. MDM morphology and actin content change with age and with loss of *MYC* or *USF1*

(A) Representative images of young and older MDMs stained with phalloidin. Scale bar, 1,000 μm.

(B–D) Morphological changes between young (N = 3, 23–25 years) and older (N = 3, 58–71 years) MDMs. Two-way ANOVA with Sidak's multiple comparison, $^{*}p < 0.05$, $^{**}p < 0.01$, $^{***}p < 0.001$, $^{****}p < 0.0001$. ns, not significant.

(E–G) Morphological changes with loss of *MYC* or *USF1* compared with control in young MDMs. $N = 4$, repeated-measures one-way ANOVA with Tukey's multiple comparison, $^{*}p < 0.05$, $^{**}p < 0.01$, $^{***}p < 0.001$, $^{****}p < 0.0001$. ns, not significant.

(legend continued on next page)

human M^0 MDMs compared with control and with age in murine BMDMs, human MDMs showed no significant difference with age in *CCR2* expression.

Mechanisms underlying downregulation of *MYC* and *USF1* in macrophages with age remain to be explored. Dysregulated metabolism and redox balance have been linked to downregulation of *Myc* in aged mice where macrophages are finely tuned to alter metabolism according to their environment.[86] It will be interesting to explore epigenetic changes that may lead to downregulation of *MYC* and *USF1* in macrophages with age in the future.

In summary, we have highlighted specific functions and key regulatory factors of *MYC* and *USF1* that decline with age in human macrophages. Importantly, the older age group, showing markedly reduced phagocytosis, migration, and chemotactic migration, were from healthy individuals over 50 years old with a mean age of 61 years. This average age is more than 20 years below the average life expectancy in countries with modern healthcare. The clear phenotypical changes seen in the relatively young age of our older cohort shows that innate immune functional decline may represent the starting point of aging, with a culmination of factors prompting age-related disease and frailty. The underlying mechanisms of human MDM aging are far from completely understood; the downstream functionally relevant targets of *MYC* and *USF1* that are also dysregulated with age will be a crucial starting point for future investigations.

Limitations of the study

Our studies using human MDMs were from two gender-balanced healthy volunteer age groups: 18–30 years (mean age 24 ± 1.2 SD years; young cohort) or >50 years (mean age 61 ± 5.7 SD years; older cohort). The healthy aging donors are without comorbidities and frailty seen in the aging human population, which will form more complex interesting future studies beyond the scope of this work. Human macrophage function was determined *in vitro*, since live phagocytosis and migration detection would not have been possible *in vivo*. Assessing function and gene expression under resting and specific stimulation conditions offers a simplified model compared to macrophages *in vivo*. Mouse macrophages were from male animals, but these were extrapolated to human macrophage assessment from gender-balanced groups.

STAR★METHODS

Detailed methods are provided in the online version of this paper and include the following:

- KEY RESOURCES TABLE
- RESOURCE AVAILABILITY
  - Lead contact
  - Materials availability
  - Data and code availability
- EXPERIMENTAL MODEL AND STUDY PARTICIPANT DETAILS
  - Mice
  - Human specimens
- METHOD DETAILS
  - Human monocyte and monocyte-derived macrophage isolation and culture
  - Functional assays
  - Phagocytosis assay
  - Scratch assay
  - MCP-1 transwell migration assay
  - Microarray analysis of murine alveolar macrophages
  - Further bioinformatic analysis of identified transcription factors
  - Murine bone marrow-derived macrophage isolation and culture
  - RNA isolation
  - Gene expression analysis by RT-qPCR
  - RNA sequencing analysis
  - Western blotting
  - Cytoskeleton staining and analysis
- QUANTIFICATION AND STATISTICAL ANALYSIS

SUPPLEMENTAL INFORMATION

Supplemental information can be found online at https://doi.org/10.1016/j.celrep.2024.114073.

ACKNOWLEDGMENTS

We thank Mark Ariaans, Jonathan Kilby, and Kay Hopkinson for technical assistance. We also thank phlebotomists Salman Almalki and Saffron Foster as well as all of the volunteers who donated blood to this research. Finally, we thank Steve Renshaw, Alison Condliffe, and Colin Bingle for their editorial input. This work was supported by the Healthy Lifespan Institute, University of Sheffield.

AUTHOR CONTRIBUTIONS

C.E.M., S.A.J., J.V.K., M.C., V.C., and S.H. performed the experiments and data analysis and wrote the manuscript. A.H.G., S.D., I.S., D.C., H.L.W., and E.K.-T. designed and supervised the study and contributed to data analysis and interpretation, as well as development and writing of the manuscript. All authors reviewed the manuscript.

DECLARATION OF INTERESTS

The authors declare no competing interests.

Received: October 27, 2023
Revised: February 15, 2024
Accepted: March 21, 2024
Published: April 4, 2024

In (B) and (E), area by square pixel of MDMs in young and older (C) and knockdown (F) conditions is shown. In (C) and (F), mean fluorescence intensity of MDMs stained with phalloidin to measure actin content in young and older (D) and knockdown (G) conditions is shown. In (D) and (G), circularity (where 1 is a perfect circle and approaching 0.0 is increasingly elongated) of MDMs in young and older (E) and knockdown (H) conditions is shown. A minimum of 100 cells per condition were analyzed across the four images. Data are presented as the mean ± SEM with each data point representing an individual donor, that is, the median (B, D, E, and G) or geometric mean (C and F) of all cells in four images taken.

REFERENCES

1. Ross, E.A., Devitt, A., and Johnson, J.R. (2021). Macrophages: the good, the bad, and the gluttony. Front. Immunol. *12*, 708186. https://doi.org/10.3389/fimmu.2021.708186.
2. Mass, E., Nimmerjahn, F., Kierdorf, K., and Schlitzer, A. (2023). Tissue-specific macrophages: how they develop and choreograph tissue biology. Nat. Rev. Immunol. *23*, 563–579. https://doi.org/10.1038/s41577-023-00848-y.
3. Franceschi, C., Garagnani, P., Parini, P., Giuliani, C., and Santoro, A. (2018). Inflammaging: a new immune–metabolic viewpoint for age-related diseases. Nat. Rev. Endocrinol. *14*, 576–590. https://doi.org/10.1038/s41574-018-0059-4.
4. Jablonski, K.A., Amici, S.A., Webb, L.M., Ruiz-Rosado, J.D., Popovich, P.G., Partida-Sanchez, S., and Guerau-de-Arellano, M. (2015). Novel markers to delineate murine M1 and M2 macrophages. PLoS One *10*, e0145342. https://doi.org/10.1371/journal.pone.0145342.
5. Franceschi, C., Bonafè, M., Valensin, S., Olivieri, F., De Luca, M., Ottaviani, E., and De Benedictis, G. (2000). Inflamm-aging: an evolutionary perspective on immunosenescence. Ann. N. Y. Acad. Sci. *908*, 244–254. https://doi.org/10.1111/j.1749-6632.2000.tb06651.x.
6. Moss, C.E., Phipps, H., Wilson, H.L., and Kiss-Toth, E. (2023). Markers of the ageing macrophage: a systematic review and meta-analysis. Front. Immunol. *14*, 1222308. https://doi.org/10.3389/fimmu.2023.1222308.
7. Takahashi, R., Totsuka, S., Ishigami, A., Kobayashi, Y., and Nagata, K. (2016). Attenuated phagocytosis of secondary necrotic neutrophils by macrophages in aged and SMP30 knockout mice. Geriatr. Gerontol. Int. *16*, 135–142. https://doi.org/10.1111/ggi.12436.
8. Linehan, E., Dombrowski, Y., Snoddy, R., Fallon, P.G., Kissenpfennig, A., and Fitzgerald, D.C. (2014). Aging impairs peritoneal but not bone marrow-derived macrophage phagocytosis. Aging Cell *13*, 699–708. https://doi.org/10.1111/acel.12223.
9. Natrajan, M.S., de la Fuente, A.G., Crawford, A.H., Linehan, E., Nuñez, V., Johnson, K.R., Wu, T., Fitzgerald, D.C., Ricote, M., Bielekova, B., and Franklin, R.J.M. (2015). Retinoid X receptor activation reverses age-related deficiencies in myelin debris phagocytosis and remyelination. Brain *138*, 3581–3597. https://doi.org/10.1093/brain/awv289.
10. Lu, R., Sampathkumar, N.K., and Benayoun, B.A. (2020). Measuring phagocytosis in bone marrow-derived macrophages and peritoneal macrophages with aging. Methods Mol. Biol. *2144*, 161–170. https://doi.org/10.1007/978-1-0716-0592-9_14.
11. Petrequin, P.R., and Johnson, A.G. (1984). Macrophage activation by adjuvants in aging mice. J. Leukoc. Biol. *35*, 251–263. https://doi.org/10.1002/jlb.35.3.251.
12. Rawji, K.S., Young, A.M.H., Ghosh, T., Michaels, N.J., Mirzaei, R., Kappen, J., Kolehmainen, K.L., Alaeiilkhchi, N., Lozinski, B., Mishra, M.K., et al. (2020). Niacin-mediated rejuvenation of macrophage/microglia enhances remyelination of the aging central nervous system. Acta Neuropathol. *139*, 893–909. https://doi.org/10.1007/s00401-020-02129-7.
13. Rawji, K.S., Kappen, J., Tang, W., Teo, W., Plemel, J.R., Stys, P.K., and Yong, V.W. (2018). Deficient surveillance and phagocytic activity of myeloid cells within demyelinated lesions in aging mice visualized by *ex vivo* live multiphoton imaging. J. Neurosci. *38*, 1973–1988. https://doi.org/10.1523/jneurosci.2341-17.2018.
14. Wong, C.K., Smith, C.A., Sakamoto, K., Kaminski, N., Koff, J.L., and Goldstein, D.R. (2017). Aging impairs alveolar macrophage phagocytosis and increases influenza-induced mortality in mice. J. Immunol. *199*, 1060–1068. https://doi.org/10.4049/jimmunol.1700397.
15. Li, Z., Jiao, Y., Fan, E.K., Scott, M.J., Li, Y., Li, S., Billiar, T.R., Wilson, M.A., Shi, X., and Fan, J. (2017). Aging-impaired filamentous actin polymerization signaling reduces alveolar macrophage phagocytosis of bacteria. J. Immunol. *199*, 3176–3186. https://doi.org/10.4049/jimmunol.1700140.
16. Fix, D.K., Ekiz, H.A., Petrocelli, J.J., Mckenzie, A.M., Mahmassani, Z.S., O'Connell, R.M., and Drummond, M.J. (2021). Disrupted macrophage metabolic reprogramming in aged soleus muscle during early recovery following disuse atrophy. Aging Cell *20*, e13448. https://doi.org/10.1111/acel.13448.
17. Hachim, D., Wang, N., Lopresti, S.T., Stahl, E.C., Umeda, Y.U., Rege, R.D., Carey, S.T., Mani, D., and Brown, B.N. (2017). Effects of aging upon the host response to implants. J. Biomed. Mater. Res. *105*, 1281–1292. https://doi.org/10.1002/jbm.a.36013.
18. Kim, O.H., Kim, H., Kang, J., Yang, D., Kang, Y.H., Lee, D.H., Cheon, G.J., Park, S.C., and Oh, B.C. (2017). Impaired phagocytosis of apoptotic cells causes accumulation of bone marrow-derived macrophages in aged mice. BMB Rep. *50*, 43–48. https://doi.org/10.5483/BMBRep.2017.50.1.167.
19. Peradinovic, J., Mohovic, N., Bulic, K., Markovinovic, A., Cimbro, R., and Munitic, I. (2023). Ageing-induced decline in primary myeloid cell phagocytosis is unaffected by optineurin insufficiency. Biology *12*, 240. https://doi.org/10.3390/biology12020240.
20. De la Fuente, M., Del Río, M., and Medina, S. (2001). Changes with aging in the modulation by neuropeptide Y of murine peritoneal macrophage functions. J. Neuroimmunol. *116*, 156–167. https://doi.org/10.1016/S0165-5728(01)00297-1.
21. Zhao, H., Roychoudhury, J., Doggett, T.A., Apte, R.S., and Ferguson, T.A. (2013). Age-dependent changes in FasL (CD95L) modulate macrophage function in a model of age-related macular degeneration. Invest. Ophthalmol. Vis. Sci. *54*, 5321–5331. https://doi.org/10.1167/iovs.13-12122.
22. Irvine, K.M., Skoien, R., Bokil, N.J., Melino, M., Thomas, G.P., Loo, D., Gabrielli, B., Hill, M.M., Sweet, M.J., Clouston, A.D., and Powell, E.E. (2014). Senescent human hepatocytes express a unique secretory phenotype and promote macrophage migration. World J. Gastroenterol. *20*, 17851–17862. https://doi.org/10.3748/wjg.v20.i47.17851.
23. Duong, L., Radley, H.G., Lee, B., Dye, D.E., Pixley, F.J., Grounds, M.D., Nelson, D.J., and Jackaman, C. (2021). Macrophage function in the elderly and impact on injury repair and cancer. Immun. Ageing *18*, 4. https://doi.org/10.1186/s12979-021-00215-2.
24. Blacher, E., Tsai, C., Litichevskiy, L., Shipony, Z., Iweka, C.A., Schneider, K.M., Chuluun, B., Heller, H.C., Menon, V., Thaiss, C.A., and Andreasson, K.I. (2022). Aging disrupts circadian gene regulation and function in macrophages. Nat. Immunol. *23*, 229–236. https://doi.org/10.1038/s41590-021-01083-0.
25. Maity, A.K., Hu, X., Zhu, T., and Teschendorff, A.E. (2022). Inference of age-associated transcription factor regulatory activity changes in single cells. Nat. Aging *2*, 548–561. https://doi.org/10.1038/s43587-022-00233-9.
26. Wu, Y., Hu, S.S., Zhang, R., Goplen, N.P., Gao, X., Narasimhan, H., Shi, A., Chen, Y., Li, Y., Zang, C., et al. (2023). Single cell RNA sequencing unravels mechanisms underlying senescence-like phenotypes of alveolar macrophages. iScience *26*, 107197. https://doi.org/10.1016/j.isci.2023.107197.
27. Davies, L.C., Jenkins, S.J., Allen, J.E., and Taylor, P.R. (2013). Tissue-resident macrophages. Nat. Immunol. *14*, 986–995. https://doi.org/10.1038/ni.2705.
28. Heinig, M., Petretto, E., Wallace, C., Bottolo, L., Rotival, M., Lu, H., Li, Y., Sarwar, R., Langley, S.R., Bauerfeind, A., et al. (2010). A trans-acting locus regulates an anti-viral expression network and type 1 diabetes risk. Nature *467*, 460–464. https://doi.org/10.1038/nature09386.
29. Rotival, M., Zeller, T., Wild, P.S., Maouche, S., Szymczak, S., Schillert, A., Castagné, R., Deiseroth, A., Proust, C., Brocheton, J., et al. (2011). Integrating genome-wide genetic variations and monocyte expression data reveals trans-regulated gene modules in humans. PLoS Genet. *7*, e1002367. https://doi.org/10.1371/journal.pgen.1002367.
30. Schunkert, H., König, I.R., Kathiresan, S., Reilly, M.P., Assimes, T.L., Holm, H., Preuss, M., Stewart, A.F.R., Barbalic, M., Gieger, C., et al. (2011). Large-scale association analysis identifies 13 new susceptibility

loci for coronary artery disease. Nat. Genet. *43*, 333–338. https://doi.org/10.1038/ng.784.

31. Wong, K.L., Tai, J.J.Y., Wong, W.C., Han, H., Sem, X., Yeap, W.H., Kourilsky, P., and Wong, S.C. (2011). Gene expression profiling reveals the defining features of the classical, intermediate, and nonclassical human monocyte subsets. Blood *118*, e16–e31. https://doi.org/10.1182/blood-2010-12-326355.

32. Frankenberger, M., Hofer, T.P.J., Marei, A., Dayyani, F., Schewe, S., Strasser, C., Aldraihim, A., Stanzel, F., Lang, R., Hoffmann, R., et al. (2012). Transcript profiling of CD16-positive monocytes reveals a unique molecular fingerprint. Eur. J. Immunol. *42*, 957–974. https://doi.org/10.1002/eji.201141907.

33. Ancuta, P., Liu, K.Y., Misra, V., Wacleche, V.S., Gosselin, A., Zhou, X., and Gabuzda, D. (2009). Transcriptional profiling reveals developmental relationship and distinct biological functions of CD16+ and CD16- monocyte subsets. BMC Genom. *10*, 403. https://doi.org/10.1186/1471-2164-10-403.

34. Kyogoku, C., Smiljanovic, B., Grün, J.R., Biesen, R., Schulte-Wrede, U., Häupl, T., Hiepe, F., Alexander, T., Radbruch, A., and Grützkau, A. (2013). Cell-specific type I IFN signatures in autoimmunity and viral infection: what makes the difference? PLoS One *8*, e83776. https://doi.org/10.1371/journal.pone.0083776.

35. Liberzon, A., Birger, C., Thorvaldsdóttir, H., Ghandi, M., Mesirov, J.P., and Tamayo, P. (2015). The molecular signatures database hallmark gene set collection. Cell Syst. *1*, 417–425. https://doi.org/10.1016/j.cels.2015.12.004.

36. Sierra-Filardi, E., Nieto, C., Domínguez-Soto, A., Barroso, R., Sánchez-Mateos, P., Puig-Kroger, A., López-Bravo, M., Joven, J., Ardavín, C., Rodríguez-Fernández, J.L., et al. (2014). CCL2 shapes macrophage polarization by GM-CSF and M-CSF: identification of CCL2/CCR2-dependent gene expression profile. J. Immunol. *192*, 3858–3867. https://doi.org/10.4049/jimmunol.1302821.

37. Rougerie, P., Miskolci, V., and Cox, D. (2013). Generation of membrane structures during phagocytosis and chemotaxis of macrophages: role and regulation of the actin cytoskeleton. Immunol. Rev. *256*, 222–239. https://doi.org/10.1111/imr.12118.

38. Onken, M.D., Blumer, K.J., and Cooper, J.A. (2021). Uveal melanoma cells use ameboid and mesenchymal mechanisms of cell motility crossing the endothelium. Mol. Biol. Cell *32*, 413–421. https://doi.org/10.1091/mbc.E20-04-0241.

39. Logue, J.S., Cartagena-Rivera, A.X., and Chadwick, R.S. (2018). c-Src activity is differentially required by cancer cell motility modes. Oncogene *37*, 2104–2121. https://doi.org/10.1038/s41388-017-0071-5.

40. Abshire, M.Y., Thomas, K.S., Owen, K.A., and Bouton, A.H. (2011). Macrophage motility requires distinct $\alpha5\beta1$/FAK and $\alpha4\beta1$/paxillin signaling events. J. Leukoc. Biol. *89*, 251–257. https://doi.org/10.1189/jlb.0710395.

41. Tang, Z., Davidson, D., Li, R., Zhong, M.C., Qian, J., Chen, J., and Veillette, A. (2021). Inflammatory macrophages exploit unconventional pro-phagocytic integrins for phagocytosis and anti-tumor immunity. Cell Rep. *37*, 110111. https://doi.org/10.1016/j.celrep.2021.110111.

42. Lee, D.Y., Lim, J.S., and Cho, K.A. (2020). Differential activation of macrophages based on their environment in advanced age. Chonnam Med. J. *56*, 12–19. https://doi.org/10.4068/cmj.2020.56.1.12.

43. Vida, C., de Toda, I.M., Cruces, J., Garrido, A., Gonzalez-Sanchez, M., and De la Fuente, M. (2017). Role of macrophages in age-related oxidative stress and lipofuscin accumulation in mice. Redox Biol. *12*, 423–437. https://doi.org/10.1016/j.redox.2017.03.005.

44. Martínez de Toda, I., Vida, C., Sanz San Miguel, L., and De la Fuente, M. (2019). Function, oxidative, and inflammatory stress parameters in immune cells as predictive markers of lifespan throughout aging. Oxid. Med. Cell. Longev. *2019*, 4574276. https://doi.org/10.1155/2019/4574276.

45. Martínez de Toda, I., Vida, C., Sanz San Miguel, L., and De la Fuente, M. (2019). When will my mouse die? Life span prediction based on immune function, redox and behavioural parameters in female mice at the adult age. Mech. Ageing Dev. *182*, 111125. https://doi.org/10.1016/j.mad.2019.111125.

46. Levens, D. (2013). Cellular MYCro economics: balancing MYC function with MYC expression. Cold Spring Harb. Perspect. Med. *3*, a014233. https://doi.org/10.1101/cshperspect.a014233.

47. Pello, O.M. (2016). Macrophages and c-Myc cross paths. OncoImmunology *5*, e1151991. https://doi.org/10.1080/2162402X.2016.1151991.

48. Martinez, F.O., Helming, L., Milde, R., Varin, A., Melgert, B.N., Draijer, C., Thomas, B., Fabbri, M., Crawshaw, A., Ho, L.P., et al. (2013). Genetic programs expressed in resting and IL-4 alternatively activated mouse and human macrophages: similarities and differences. Blood *121*, e57–e69. https://doi.org/10.1182/blood-2012-06-436212.

49. Pello, O.M., De Pizzol, M., Mirolo, M., Soucek, L., Zammataro, L., Amabile, A., Doni, A., Nebuloni, M., Swigart, L.B., Evan, G.I., et al. (2012). Role of c-MYC in alternative activation of human macrophages and tumor-associated macrophage biology. Blood *119*, 411–421. https://doi.org/10.1182/blood-2011-02-339911.

50. Duffy, M.J., O'Grady, S., Tang, M., and Crown, J. (2021). MYC as a target for cancer treatment. Cancer Treat Rev. *94*, 102154. https://doi.org/10.1016/j.ctrv.2021.102154.

51. Meyer, N., and Penn, L.Z. (2008). Reflecting on 25 years with MYC. Nat. Rev. Cancer *8*, 976–990. https://doi.org/10.1038/nrc2231.

52. Takahashi, K., and Yamanaka, S. (2006). Induction of pluripotent stem cells from mouse embryonic and adult fibroblast cultures by defined factors. Cell *126*, 663–676. https://doi.org/10.1016/j.cell.2006.07.024.

53. Ocampo, A., Reddy, P., Martinez-Redondo, P., Platero-Luengo, A., Hatanaka, F., Hishida, T., Li, M., Lam, D., Kurita, M., Beyret, E., et al. (2016). In Vivo Amelioration of Age-Associated Hallmarks by Partial Reprogramming. Cell *167*, 1719–1733.e12. https://doi.org/10.1016/j.cell.2016.11.052.

54. Yuan, J., Minter-Dykhouse, K., and Lou, Z. (2009). A c-Myc–SIRT1 feedback loop regulates cell growth and transformation. J. Cell Biol. *185*, 203–211. https://doi.org/10.1083/jcb.200809167.

55. Ahuja, P., Zhao, P., Angelis, E., Ruan, H., Korge, P., Olson, A., Wang, Y., Jin, E.S., Jeffrey, F.M., Portman, M., and Maclellan, W.R. (2010). Myc controls transcriptional regulation of cardiac metabolism and mitochondrial biogenesis in response to pathological stress in mice. J. Clin. Invest. *120*, 1494–1505. https://doi.org/10.1172/JCI38331.

56. Kumari, A., Folk, W.P., and Sakamuro, D. (2017). The dual roles of MYC in genomic instability and cancer chemoresistance. Genes *8*, 158. https://doi.org/10.3390/genes8060158.

57. López-Otín, C., Blasco, M.A., Partridge, L., Serrano, M., and Kroemer, G. (2013). The hallmarks of aging. Cell *153*, 1194–1217. https://doi.org/10.1016/j.cell.2013.05.039.

58. Macedo, J.C., Vaz, S., Bakker, B., Ribeiro, R., Bakker, P.L., Escandell, J.M., Ferreira, M.G., Medema, R., Foijer, F., and Logarinho, E. (2018). FoxM1 repression during human aging leads to mitotic decline and aneuploidy-driven full senescence. Nat. Commun. *9*, 2834. https://doi.org/10.1038/s41467-018-05258-6.

59. Fischer, M., Grossmann, P., Padi, M., and DeCaprio, J.A. (2016). Integration of TP53, DREAM, MMB-FOXM1 and RB-E2F target gene analyses identifies cell cycle gene regulatory networks. Nucleic Acids Res. *44*, 6070–6086. https://doi.org/10.1093/nar/gkw523.

60. Laurila, P.P., Soronen, J., Kooijman, S., Forsström, S., Boon, M.R., Surakka, I., Kaiharju, E., Coomans, C.P., Van Den Berg, S.A.A., Autio, A., et al. (2016). USF1 deficiency activates brown adipose tissue and improves cardiometabolic health. Sci. Transl. Med. *8*, 323ra13. https://doi.org/10.1126/scitranslmed.aad0015.

61. Zhou, Y., Zhao, Y., Ma, W., Zhang, L., Jiang, Y., and Dong, W. (2022). USF1-CHCHD4 axis promotes lung adenocarcinoma progression partially

via activating the MYC pathway. Discov. Oncol. *13*, 136. https://doi.org/10.1007/s12672-022-00600-3.

62. Naukkarinen, J., Gentile, M., Soro-Paavonen, A., Saarela, J., Koistinen, H.A., Pajukanta, P., Taskinen, M.R., and Peltonen, L. (2005). USF1 and dyslipidemias: converging evidence for a functional intronic variant. Hum. Mol. Genet. *14*, 2595–2605. https://doi.org/10.1093/hmg/ddi294.
63. Pajukanta, P., Lilja, H.E., Sinsheimer, J.S., Cantor, R.M., Lusis, A.J., Gentile, M., Duan, X.J., Soro-Paavonen, A., Naukkarinen, J., Saarela, J., et al. (2004). Familial combined hyperlipidemia is associated with upstream transcription factor 1 (USF1). Nat. Genet. *36*, 371–376. https://doi.org/10.1038/ng1320.
64. Coon, H., Xin, Y., Hopkins, P.N., Cawthon, R.M., Hasstedt, S.J., and Hunt, S.C. (2005). Upstream stimulatory factor 1 associated with familial combined hyperlipidemia, LDL cholesterol, and triglycerides. Hum. Genet. *117*, 444–451. https://doi.org/10.1007/s00439-005-1340-x.
65. Zheng, P.F., Chen, L.Z., Pan, H.W., Liu, P., and Zheng, Z.F. (2022). Effects of USF1 SNPs and SNP–environment interactions on serum lipid profiles and the risk of early-onset coronary artery disease in the Chinese population. Front. Cardiovasc. Med. *9*, 882728. https://doi.org/10.3389/fcvm.2022.882728.
66. Isotalo, K., Kok, E.H., Luoto, T.M., Haikonen, S., Haapasalo, H., Lehtimäki, T., and Karhunen, P.J. (2012). Upstream transcription factor 1 (USF1) polymorphisms associate with Alzheimer's Disease-related neuropathological lesions: Tampere autopsy study. Brain Pathol. *22*, 765–775. https://doi.org/10.1111/j.1750-3639.2012.00586.x.
67. Snodgrass, R.G., Jiang, X., and Stephensen, C.B. (2022). Monocyte subsets display age-dependent alterations at fasting and undergo non-age-dependent changes following consumption of a meal. Immun. Ageing *19*, 41. https://doi.org/10.1186/s12979-022-00297-6.
68. Seidler, S., Zimmermann, H.W., Bartneck, M., Trautwein, C., and Tacke, F. (2010). Age-dependent alterations of monocyte subsets and monocyte-related chemokine pathways in healthy adults. BMC Immunol. *11*, 30. https://doi.org/10.1186/1471-2172-11-30.
69. Teschendorff, A.E., and Wang, N. (2020). Improved detection of tumor suppressor events in single-cell RNA-Seq data. NPJ Genom. Med. *5*, 43. https://doi.org/10.1038/s41525-020-00151-y.
70. Mylvaganam, S., Freeman, S.A., and Grinstein, S. (2021). The cytoskeleton in phagocytosis and macropinocytosis. Curr. Biol. *31*, R619–R632. https://doi.org/10.1016/j.cub.2021.01.036.
71. Flannagan, R.S., Harrison, R.E., Yip, C.M., Jaqaman, K., and Grinstein, S. (2010). Dynamic macrophage "probing" is required for the efficient capture of phagocytic targets. J. Cell Biol. *191*, 1205–1218. https://doi.org/10.1083/jcb.201007056.
72. Zhou, J.Y., Szasz, T.P., Stewart-Hutchinson, P.J., Sivapalan, J., Todd, E.M., Deady, L.E., Cooper, J.A., Onken, M.D., and Morley, S.C. (2016). L-Plastin promotes podosome longevity and supports macrophage motility. Mol. Immunol. *78*, 79–88. https://doi.org/10.1016/j.molimm.2016.08.012.
73. Noble, K.V., Liu, T., Matthews, L.J., Schulte, B.A., and Lang, H. (2019). Age-related changes in immune cells of the human cochlea. Front. Neurol. *10*, 895. https://doi.org/10.3389/fneur.2019.00895.
74. Kezic, J.M., Chrysostomou, V., McMenamin, P.G., and Crowston, J.G. (2020). Effects of age on retinal macrophage responses to acute elevation of intraocular pressure. Exp. Eye Res. *193*, 107995. https://doi.org/10.1016/j.exer.2020.107995.
75. Lee, V., Rekhi, E., Hoh Kam, J., and Jeffery, G. (2012). Vitamin D rejuvenates aging eyes by reducing inflammation, clearing amyloid beta and improving visual function. Neurobiol. Aging *33*, 2382–2389. https://doi.org/10.1016/j.neurobiolaging.2011.12.002.
76. Frye, M.D., Yang, W., Zhang, C., Xiong, B., and Hu, B.H. (2017). Dynamic activation of basilar membrane macrophages in response to chronic sensory cell degeneration in aging mouse cochleae. Hear. Res. *344*, 125–134. https://doi.org/10.1016/j.heares.2016.11.003.
77. Benedusi, V., Meda, C., Della Torre, S., Monteleone, G., Vegeto, E., and Maggi, A. (2012). A lack of ovarian function increases neuroinflammation in aged mice. Endocrinology *153*, 2777–2788. https://doi.org/10.1210/en.2011-1925.
78. Rozovsky, I., Finch, C.E., and Morgan, T.E. (1998). Age-related activation of microglia and astrocytes: in vitro studies show persistent phenotypes of aging, increased proliferation, and resistance to down-regulation. Neurobiol. Aging *19*, 97–103. https://doi.org/10.1016/S0197-4580(97)00169-3.
79. Iiyama, M., Shimada, Y., Kita, T., and Ito, H. (1992). Effect of aging on macrophage adherence to extracellular matrix proteins. Mech. Ageing Dev. *66*, 149–158. https://doi.org/10.1016/0047-6374(92)90132-W.
80. Babagana, M., Oh, K.S., Chakraborty, S., Pacholewska, A., Aqdas, M., and Sung, M.H. (2021). Hedgehog dysregulation contributes to tissue-specific inflammaging of resident macrophages. Aging (Albany NY) *13*, 19207–19229. https://doi.org/10.18632/aging.203422.
81. Mohamed, F., Mansfield, B.S., and Raal, F.J. (2022). ANGPTL3 as a drug target in hyperlipidemia and atherosclerosis. Curr. Atherosclerosis Rep. *24*, 959–967. https://doi.org/10.1007/s11883-022-01071-1.
82. Manta, C.P., Leibing, T., Friedrich, M., Nolte, H., Adrian, M., Schledzewski, K., Krzistetzko, J., Kirkamm, C., David Schmid, C., Xi, Y., et al. (2022). Targeting of scavenger receptors stabilin-1 and stabilin-2 ameliorates atherosclerosis by a plasma proteome switch mediating monocyte/macrophage suppression. Circulation *146*, 1783–1799. https://doi.org/10.1161/circulationaha.121.058615.
83. Yang, W.J., Cao, R.C., Xiao, W., Zhang, X.L., Xu, H., Wang, M., Zhou, Z.T., Chen, H.J., Xu, J., Chen, X.M., et al. (2022). Acinar ATP8b1/LPC pathway promotes macrophage efferocytosis and clearance of inflammation during chronic pancreatitis development. Cell Death Dis. *13*, 893. https://doi.org/10.1038/s41419-022-05322-6.
84. Takaya, K., Asou, T., and Kishi, K. (2022). Downregulation of senescence-associated secretory phenotype by knockdown of secreted frizzled-related protein 4 contributes to the prevention of skin aging. Aging (Albany NY) *14*, 8167–8178. https://doi.org/10.18632/aging.204273.
85. Onishi, Y., Fukasawa, K., Ozaki, K., Iezaki, T., Yoneda, Y., and Hinoi, E. (2016). GDF1 is a novel mediator of macrophage infiltration in brown adipose tissue of obese mice. Biochem. Biophys. Rep. *5*, 216–223. https://doi.org/10.1016/j.bbrep.2015.12.008.
86. Wang, H., Lu, J., Stevens, T., Roberts, A., Mandel, J., Avula, R., Ma, B., Wu, Y., Wang, J., Land, C.V., et al. (2023). Premature aging and reduced cancer incidence associated with near-complete body-wide Myc inactivation. Cell Rep. *42*, 112830. https://doi.org/10.1016/j.celrep.2023.112830.
87. Pollitt, E.J.G., Szkuta, P.T., Burns, N., and Foster, S.J. (2018). Staphylococcus aureus infection dynamics. PLoS Pathog. *14*, e1007112. https://doi.org/10.1371/journal.ppat.1007112.
88. Chen, E.Y., Tan, C.M., Kou, Y., Duan, Q., Wang, Z., Meirelles, G.V., Clark, N.R., and Ma'ayan, A. (2013). Enrichr: interactive and collaborative HTML5 gene list enrichment analysis tool. BMC Bioinf. *14*, 128. https://doi.org/10.1186/1471-2105-14-128.
89. Kuleshov, M.V., Jones, M.R., Rouillard, A.D., Fernandez, N.F., Duan, Q., Wang, Z., Koplev, S., Jenkins, S.L., Jagodnik, K.M., Lachmann, A., et al. (2016). Enrichr: a comprehensive gene set enrichment analysis web server 2016 update. Nucleic Acids Res. *44*, W90–W97. https://doi.org/10.1093/nar/gkw377.
90. Xie, Z., Bailey, A., Kuleshov, M.V., Clarke, D.J.B., Evangelista, J.E., Jenkins, S.L., Lachmann, A., Wojciechowicz, M.L., Kropiwnicki, E., Jagodnik, K.M., et al. (2021). Gene set knowledge discovery with Enrichr. Curr. Protoc. *1*, e90. https://doi.org/10.1002/cpz1.90.
91. Ghoussaini, M., Mountjoy, E., Carmona, M., Peat, G., Schmidt, E.M., Hercules, A., Fumis, L., Miranda, A., Carvalho-Silva, D., Buniello, A., et al. (2021). Open Targets Genetics: systematic identification of trait-associated genes using large-scale genetics and functional genomics. Nucleic Acids Res. *49*, D1311–D1320. https://doi.org/10.1093/nar/gkaa840.

92. Mountjoy, E., Schmidt, E.M., Carmona, M., Schwartzentruber, J., Peat, G., Miranda, A., Fumis, L., Hayhurst, J., Buniello, A., Karim, M.A., et al. (2021). An open approach to systematically prioritize causal variants and genes at all published human GWAS trait-associated loci. Nat. Genet. *53*, 1527–1533. https://doi.org/10.1038/s41588-021-00945-5.

93. Staley, J.R., Blackshaw, J., Kamat, M.A., Ellis, S., Surendran, P., Sun, B.B., Paul, D.S., Freitag, D., Burgess, S., Danesh, J., et al. (2016). PhenoScanner: a database of human genotype-phenotype associations. Bioinformatics *32*, 3207–3209. https://doi.org/10.1093/bioinformatics/btw373.

94. Kamat, M.A., Blackshaw, J.A., Young, R., Surendran, P., Burgess, S., Danesh, J., Butterworth, A.S., and Staley, J.R. (2019). PhenoScanner V2: an expanded tool for searching human genotype-phenotype associations. Bioinformatics *35*, 4851–4853. https://doi.org/10.1093/bioinformatics/btz469.

95. Dobin, A., Davis, C.A., Schlesinger, F., Drenkow, J., Zaleski, C., Jha, S., Batut, P., Chaisson, M., and Gingeras, T.R. (2013). STAR: ultrafast universal RNA-seq aligner. Bioinformatics *29*, 15–21. https://doi.org/10.1093/bioinformatics/bts635.

96. Mootha, V.K., Lindgren, C.M., Eriksson, K.F., Subramanian, A., Sihag, S., Lehar, J., Puigserver, P., Carlsson, E., Ridderstråle, M., Laurila, E., et al. (2003). PGC-1α-responsive genes involved in oxidative phosphorylation are coordinately downregulated in human diabetes. Nat. Genet. *34*, 267–273. https://doi.org/10.1038/ng1180.

97. Subramanian, A., Tamayo, P., Mootha, V.K., Mukherjee, S., Ebert, B.L., Gillette, M.A., Paulovich, A., Pomeroy, S.L., Golub, T.R., Lander, E.S., and Mesirov, J.P. (2005). Gene set enrichment analysis: a knowledge-based approach for interpreting genome-wide expression profiles. Proc. Natl. Acad. Sci. USA *102*, 15545–15550. https://doi.org/10.1073/pnas.0506580102.

98. Eden, E., Lipson, D., Yogev, S., and Yakhini, Z. (2007). Discovering motifs in ranked lists of DNA sequences. PLoS Comput. Biol. *3*, e39. https://doi.org/10.1371/journal.pcbi.0030039.

99. Eden, E., Navon, R., Steinfeld, I., Lipson, D., and Yakhini, Z. (2009). GOrilla: a tool for discovery and visualization of enriched GO terms in ranked gene lists. BMC Bioinf. *10*, 48. https://doi.org/10.1186/1471-2105-10-48.

STAR★METHODS

KEY RESOURCES TABLE

REAGENT or RESOURCE	SOURCE	IDENTIFIER
Antibodies		
Rabbit monoclonal anti-c-myc	Cell Signaling Technology	CAT#: 5605; RRID: AB_1903938
Mouse monoclonal anti-α-tubulin	Cell Signaling Technology	CAT#: 3873; RRID: AB_1904178
Anti-rabbit IgG, HRP-linked	Cell Signaling Technology	CAT#: 7074; RRID: AB_2099233
Anti-mouse IgG, HRP-linked	Cell Signaling Technology	CAT#: 7076; RRID: AB_330924
Bacterial and virus strains		
Staphylococcus aureus	Pollitt et al.[87]	N/A
Biological samples		
Human monocyte-derived macrophages	Volunteer blood	N/A
Mouse bone marrow-derived macrophages	University of Sheffield BSU	N/A
Chemicals, peptides, and recombinant proteins		
M-CSF	Peprotech	CAT#: 300-25-100
LPS	Enzo	CAT#: ALX-581-007-L001
Ficoll-Paque PLUS media	GE Healthcare	CAT#: 11778538
IFN-γ	Peprotech	CAT#: 300-02
IL-4	Peprotech	CAT#: 200-04
Fugene HD	Promega	CAT#: E2311
RPMI1640	Gibco	CAT#: 31870-074
DMEM	Gibco	CAT#: 11965092
Opti-MEM reduced serum medium	Gibco	CAT#: 31985070
FBS Good	Pan Biotech	CAT#: P40-37100M
Penicillin-Streptomycin	Gibco	CAT#: P4458-100ML
L-Glutamine	Lonza Bioscience	CAT#: BE17-605E
Human CD14 microbeads	Miltenyi Biotec	CAT#: 130-050-201
Fluoresbrite YG microspheres 1.00 μm	Polysciences	CAT#: 17154-10
Human MCP-1	Peprotech	CAT#: 300-04-5uG
ON-TARGET plus smartpool siRNA Human *MYC*	Dharmacon	CAT#: L-003282-02-0005
ON-TARGET plus smartpool siRNA Human *USF1*	Dharmacon	CAT#: L-003617-00-0005
ON-TARGET plus smartpool control non-targeting siRNA	Dharmacon	CAT#: D-001810-10-20
Fluorescein Isothiocyanate labeled Phalloidin	Sigma-Aldrich	CAT#: P5282
PKH26 red fluorescent cell linker	Sigma-Aldrich	CAT#: PKH26GL
4% formaldehyde	Fisher Scientific	CAT#: 15413179
4% paraformaldehyde	Fisher Scientific	CAT#: 15670799
Critical commercial assays		
SYBR Green PCR Master Mix	Primer Design	CAT#: Z-PPLUS_SY10-ML
iScript cDNA synthesis kit	BIO-RAD	CAT#: 1708891
ReliaPrep RNA Cell Miniprep system	Promega	CAT#: Z6011
Deposited data		
Human monocyte-derived macrophage sequencing data	This paper	GEO: GSE240075
Oligonucleotides		
qRT-PCR primers for human and mouse	Table S4	N/A
Software and algorithms		
ImageJ v2.9.0	ImageJ	N/A
GraphPad Prism8 v10.1.0	GraphPad	N/A
NIS-Elements Viewer v5.21	NIS-Elements Viewer	N/A

(*Continued on next page*)

Continued

REAGENT or RESOURCE	SOURCE	IDENTIFIER
R v4.2.3	R	N/A
GSEA v4.2.3	GSEA	N/A
Other		
Cardiogenics Consortium transcriptomic study	Heinig et al., Rotival et al., Shunkert et al.[28–30]	N/A
Microarray analysis of murine alveolar macrophage aging	Wong et al.[14]	GEO: GSE84901

RESOURCE AVAILABILITY

Lead contact

Further information and requests for resources and reagents should be directed to and will be fulfilled by the lead contact, Endre Kiss-Toth (e.kiss-toth@sheffield.ac.uk).

Materials availability

This study did not generate new unique reagents.

Data and code availability

RNA-seq data have been deposited in GEO under accession number GSE240075 and are publicly available as of the date of publication. Microscopy data reported in this paper will be shared by the lead contact upon request. All original code has been deposited in GitHub and is publicly available as of the date of publication. Any additional information required to reanalyze the data reported in this paper is available from the lead contact upon request.

EXPERIMENTAL MODEL AND STUDY PARTICIPANT DETAILS

Mice

C57BL6 male mice (WT) were used at 2–5 months or 22 months of age for experiments. All animal experiments were approved by the University of Sheffield Project Review Committee and performed in accordance with UK Home Office Project Licence P5395C858.

Human specimens

Peripheral blood mononuclear cells (PBMCs) were isolated from healthy sex-balanced donors in accordance with ethics approved by the University of Sheffield ethics committee (031330). All blood donors gave informed consent and studies were performed in accordance with the regulations of the local ethics committee.

METHOD DETAILS

Human monocyte and monocyte-derived macrophage isolation and culture

Blood was drawn by venepuncture and mixed with 3.8% (w/v) trisodium citrate ($Na_3C_6O_7$). Blood was then layered onto Ficoll-Paque PLUS (GE Healthcare) and gradient centrifugation performed. Peripheral blood mononuclear cells were separated into phosphate buffer saline (PBS) containing 2mM ethylenediaminetetraacetic acid (EDTA) and red blood cells were lysed using a solution of ammonium chloride (155 mM NH_4Cl, 10 mM $KHCO_3$, 0.1 M EDTA in H_2O). Positive selection of human monocytes was performed using magnetic CD14 microbeads (Miltenyi Biotec). Isolated monocytes were incubated in RPMI 1640 medium (Gibco) containing 10% (v/v) heat-inactivated fetal bovine serum (HI-FBS), 1% (v/v) L-Glutamine (Lonza), 1% (v/v) penicillin-streptomycin (Gibco) and 100 nM macrophage colony stimulating factor (M-CSF) (Peprotech) for 7 days at 37°C and 5% CO_2. Differentiated monocyte-derived macrophages (MDMs) were then left unstimulated (M^0), polarized toward an inflammatory phenotype using 100 nM lipopolysaccharide (LPS) (Enzo) and 20nM interferon-γ (IFNγ) (Peprotech) ($M^{LPS+IFN\gamma}$) or polarized toward an anti-inflammatory phenotype using 20nM interleukin 4 (IL-4) (Peprotech) for a further 24 h. Small interfering RNAs were transfected into differentiated macrophages to achieve RNA silencing prior to stimulation where applicable. Transfection reagent Fugene HD (Promega) was used following manufacturer's instructions. siRNA targeting *MYC* gene (ON-TARGET plus smartpool siRNA #L-003282-02, Dharmacon) or *USF1* gene (ON-TARGET plus smartpool siRNA #L-003617, Dharmacon) was mixed at 12.5 nM with transfection reagent and Opti-MEM (Gibco). As a control, ON-TARGET plus smartpool control non-targeting (NT) siRNA (#D-001810-10-20, Dharmacon) was used at the same concentration with transfection reagent.

Functional assays

Functional assays were performed on human monocytes and MDMs under the following conditions: young M^0 and $M^{LPS+IFN\gamma}$, older M^0 and $M^{LPS+IFN\gamma}$, and young non-targeting siRNA (M^0 and $M^{LPS+IFN\gamma}$), si*USF1*-knockdown (M^0 and $M^{LPS+IFN\gamma}$) and si*MYC*-knockdown (M^0 only).

Phagocytosis assay

For phagocytosis assay, human MDMs were cultured in 12-well plates in 1 mL of media at a density of 500,000 cells per mL with a 4°C control and 37°C active plate. Fluoresbrite YG microspheres 1.00 μm (Polysciences) were opsonized with heat-inactivated FBS (Pan Biotech) for 30 min at 37°C. Five minutes before the end of incubation, control hMDMs were placed on ice. Beads were then added to each well at a concentration of 50 μL/mL and cells were incubated at 4°C or 37°C for 3 h. For phagocytosis of beads or *Staphylococcus aureus* by monocytes, 500 mL of cells were immediately seeded into 24-well plates at a density of 500,000 cells per mL in antibiotic-free RPMI media. Beads were added at the same concentration as for MDMs, while mCherry expressing *S. aureus* strain SH1000[87] were added to the cells at a multiplicity of infection of 10 and cells were again incubated at 4°C or 37°C for 3 h. After 3 h, cells were washed with PBS and fixed with 4% paraformaldehyde (PFA; Fisher Scientific) for 30 min at room temperature. Cells were washed again with PBS and stored in PBS at 4°C until microscopy. Images were taken using ZOE Fluorescent cell imager (BIO-RAD) at 20x zoom, with a brightfield (Gain: 5, Exposure: 340 ms, LED intensity: 59, Contrast: 20) and green channel (Gain: 40, Exposure: 500 ms, LED intensity: 43, Contrast: 0) or red channel (gain: 60, exposure: 500, LED intensity: 72, contrast: 0) image being taken of each field, and 3 fields being taken per temperature, condition and donor. Images were analyzed using ImageJ software v2.9.0/1.53t. The same threshold was set for each brightfield image which were then converted to mask. ''Analyze particles'' command was used to create regions of interest (ROIs) around each cell. ROIs were then overlaid onto GFP image and mean gray value was calculated for each cell. The geometric mean was then calculated for each field and normalized to the corresponding 4°C image. An average was then taken for each donor condition.

Scratch assay

To assess changes in migration, a scratch assay was performed on human MDMs cultured in 12-well plates in 1 mL of media at a density of 500,000 cells per mL. A scratch was made from the top to the bottom of the well, cells were washed with PBS and fresh media was added. Brightfield images (Gain: 5, Exposure: 340 ms, LED intensity: 59, Contrast: 20) were then immediately taken of the scratch to set a 0 h threshold number of cells in the scratch. Five fields of view were taken per condition and donor. Cells were then returned to the incubator for 6 h, from which point images were taken every 2 h to the same specification until a 14 h image was taken. For analysis of number of cells returning to the scratch, a box was drawn around the scratch at hour 0 and copied onto all other images taken of the same scratch. The cells inside the box were then counted and an average was taken from all fields at each timepoint for each donor. This was normalized back to hour 0 by subtracting the number of cells in the box at the start.

MCP-1 transwell migration assay

In order to assess ability to move toward stimuli, a transwell migration assay was performed using chemokine MCP-1. Human MDMs were cultured in 6-well plates in 2 mL of media at a density of 500,000 cells per mL and then collected using a cell scraper. Monocytes were isolated and counted immediately to the same concentration. These were centrifuged at 4000 g for 5 min and stained using PKH26 red fluorescent cell linker (Sigma-Aldrich) to better visualize the cell membrane, according to the manufacturer's instructions. 1% BSA was then added to the cells to remove excess dye and these were centrifuged again at 4000 g for 5 min. Cells were then resuspended at a density of 1 million cells per mL in 300 μL RPMI (enough to run each sample in triplicate). Using HTS Transwell 96-well permeable support, 100 μL of 1% (v/v) MCP-1 in RPMI was added to the bottom plate and 100 μL of cell suspension to the transwell insert. This was incubated for 3 h at 37°C and 5% CO_2. After 3 h, the transwell insert was removed and the bottom plate was imaged using ZOE Fluorescent cell imager (BIO-RAD) at 20x zoom, with a brightfield (Gain: 5, Exposure: 340 ms, LED intensity: 59, Contrast: 20) and Red channel (Gain: 40, Exposure: 500 ms, LED intensity: 50, Contrast: 0) image being taken of each field, and 3 fields being taken per sample. ImageJ v2.9.0/1.53t was then used to analyze each image by measuring overall mean gray value of the field and taking an average for each donor condition.

Microarray analysis of murine alveolar macrophages

The published dataset GSE84901,[14] was re-analyzed in order to assess transcription factors driving differential expression of genes with age. The pipeline for this analysis can be found in Figure S2 and is deposited at https://github.com/cemoss1/Moss_et_al/blob/main/GSE84901_pipeline.R. The dataset is comprised of microarray analysis of alveolar macrophages from young (2–4 months) and old (22–24 months) C57BL/6J mice. The infection-challenged samples were removed allowing for analysis of the differentially expressed genes (DEGs) as a direct result of aging. Significant DEGs were extracted using limma package in R v3.46.0 and defined by adjusted p value <0.05 and fold change >1.5 (upregulated with age) or < -1.5 (downregulated with age). A heatmap showing these DEGs can be found in Figure S2. These DEGs were then separated into two lists: genes upregulated with age and genes downregulated with age and these were used as input files for EnrichR analysis (https://maayanlab.cloud/Enrichr/accessed on 13.09.23)[88–90] with the full set of expressed genes in these samples used as background list. ENCODE and ChEA Consensus TFs from ChIP-X library was used to establish transcription factors likely governing their dysregulation.

Further bioinformatic analysis of identified transcription factors

The transcription factors identified as governing DEGs with age were searched for in the original DEG lists and those that were differentially expressed in the same direction as their differentially expressed target genes were taken forward. The published dataset Cardiogenics Consortium transcriptomic study,[28–30] comprising 596 donor MDMs (cultured *in vitro* in the same way as the M^0 MDMs in this study) and monocyte transcriptional profiles (Illumina's Human Ref-8 Sentrix Bead Chip arrays, Illumina Inc., San Diego, CA), was re-analyzed by ranking donors by age and comparing the top and bottom age quartiles (age range of 42–65) to assess age-related DEGs. For both *MYC* and *USF1*, the Cardiogenic Consortium study was also used to extract eQTLs present within monocytes and macrophages. These eQTLs were previously identified and made available, as described in Rotival et al..[29] They were then plotted using the locus zoom webserver to visualize LD relationships between associated SNPs and identify discrete, independent signals. To expand this, we further explored publicly available databases, including Open Target (https://genetics.opentargets.org/accessed on 13.09.23)[91,92] and Phenoscanner (http://www.phenoscanner.medschl.cam.ac.uk/accessed on 13.09.23),[93,94] to identify further *cis*-located SNPs associated with expression changes in *MYC* and *USF1* at $P < 5x10^{-8}$. Independent eQTL signals were identified using a pragmatic LD threshold ($r^2 < 0.6$), determined using the CEU population within LD Link. eQTL associated SNPs from each signal were then used to search databases for association with other phenotypes and diseases. Further, *MYC* and *USF1* putative targets within the age-related DEGs (FDR <0.05) in this dataset were assessed using the target gene library compiled on Enrichr: ENCODE and ChEA Consensus TFs from ChIP-X library (https://maayanlab.cloud/Enrichr/accessed on 31.10.23). Transcription factor targets were compared against DEGs for monocytes and macrophages separately and the percentage of DEGs that were also target genes was measured. This method of assessing putative targets in the DEGs was also completed for GSE111382 and GSE100905 datasets. Finally, the Cardiogenics Consortium transcriptomic study dataset was used to compare expression profiles between top and bottom quartiles of donor MYC expression. Gene expression analysis was carried out between top and bottom quartiles of MYC expression in the macrophage samples and genes with significant fold change were selected (FDR <0.05). The direction of comparison for this was low expression - high expression. Gene set enrichment was then performed on webgestalt online tool (https://www.webgestalt.org/accessed on 07.01.23) with community-contributed Hallmark50 database.

In order to assess *MYC* and *USF1* expression in different monocyte subsets, GEO was searched for high-throughput datasets that directly compared classical and non-classical monocytes. Four datasets were found to do this (GSE2591, GSE18565, GSE16836 and GSE51997) and the GEO database was utilized to pull out raw expression values of *MYC* and *USF1* as well as *PUM1* that has been used throughout as a reference gene. Expression of *MYC* and *USF1* was then normalized to *PUM1* by dividing each donors *MYC*/*USF1* expression by the expression of *PUM1* in that monocyte subset. This method of normalization was used as a way to compare each dataset without the need to consider batch effect.

Murine bone marrow-derived macrophage isolation and culture

All experiments on mouse samples were performed in accordance with UK legislation under the Animals (Scientific Procedures) Act 1996. Mouse leg bones were gifted to this research where they were not needed for other research purposes.

Bone marrow was isolated from femurs and tibias of young (2–5 months) and old (20–22 months) male C57BL/6J mice under aseptic conditions. Bones were flushed with DMEM (Gibco) using a syringe and 25-guage needle. The cell suspension was then passed through a 40 μm cell strainer and centrifuged at 500 *g* for 5 min. Samples obtained could then be resuspended in 90% (v/v) HI-FBS and 1-% (v/v) DMSO and frozen or immediately cultured in DMEM containing 10% (v/v) HI-FBS, 10% (v/v) L929-conditioned (M-CSF rich) media and 1% (v/v) penicillin-streptomycin (Gibco) for 5 days at 37°C and 5% CO_2. Differentiated bone marrow-derived macrophages (BMDMs) were left unstimulated or polarized in the same way as in hMDMs.

RNA isolation

Cells were first lysed in BL + TG buffer and RNA isolation was performed using ReliaPrep RNA Cell Miniprep System (Promega) according to the manufacturer's instructions. RNA was extracted from non-targeting siRNA (M^0 and $M^{LPS+IFN\gamma}$), si*USF1*-knockdown (M^0 and $M^{LPS+IFN\gamma}$) and si*MYC*-knockdown (M^0 only) hMDMs from 6 separate donors for RNA sequencing analysis.

Gene expression analysis by RT-qPCR

Following RNA isolation, concentration and purity was assessed using a NanoDrop. 100 ng total RNA per reaction was transcribed to cDNA using iScript cDNA synthesis kit (BIO-RAD), according to manufacturer's instructions. Real time qPCR was performed using CFX384 C1000 Touch Thermal Cycler (BIO-RAD) and samples were assayed using Precision PLUS SYBR-Green mastermix (Primer design). Specific genes were analyzed using primers designed using NCBI BLAST tool. Primer sequences can be found in Supplementary Table S4. All assays were performed in triplicate and normalized to expression levels of housekeeping genes $M^{LPS+IFN\gamma}$ (human) or Mau2 (mouse), as these were determined to be the most suitable across young and old samples. Relative transcript levels were analyzed using $2^{-\Delta Ct}$ method.

RNA sequencing analysis

Total RNA was isolated as previously described. An indexed pair–end sequencing run of 2 × 51 cycles on Illumina HiSeq 2000 was performed on all samples by Novogene. FASTQ files were provided which were mapped onto build 38 of the human genome using

STAR.[95] The pipeline for analysis of RNAseq data is available at: https://github.com/cemoss1/Moss_et_al/blob/main/RNAseq_pipeline.R. Mapped transcripts were then converted to genes using tximportData in R v1.18.0. Using edgeR v3.32.1, counts per million were computed and used for principal component analysis (PCA). Pairwise differential gene expression analyses for each of the comparisons were performed using DESeq2 in R v1.30.1 with non-targeting siRNA M^0 or $M^{LPS+IFN\gamma}$ control used as the reference for gene knockdown in M^0 or $M^{LPS+IFN\gamma}$, respectively. DEGs were identified using False Discovery Rate (FDR) of <5%. Gene set enrichment analysis (GSEA) v4.2.3[96,97], Enrichr (https://maayanlab.cloud/Enrichr/accessed on 31.10.23)[88–90] and GOrilla (https://cbl-gorilla.cs.technion.ac.il/accessed on 03.05.23)[98,99] analysis were performed on the DEG lists to output associated pathways.

Western blotting

Human MDMs were lysed in RIPA buffer with 1% protease inhibitor cocktail then added to Laemmeli buffer (9% (w/v) SDS, 9% (v/v) β-mercaptoethanol, 50% (v/v) glycerol in 375mM Tris-HCL, pH 6.8, 0.03% bromophenol blue) and boiled at 99°C for 10 min. Protein was then resolved on a 4–12% bis-tris gel (Invitrogen) in MES buffer at 120V for 80 min. Proteins were then transferred onto a PVDF membrane at 35V for 1 h at room temperature. After blocking for 1 h in 5% (w/v) milk in Tris-buffered saline (1% (v/v) Tween) (TBS-T) or 5% (w/v) BSA TBS-T, membranes were incubated with primary antibodies overnight at 4°C. Blots were washed 3 times in TBS-T with rolling then incubated for 1 h with HRP-conjugated secondary antibodies at room temperature. Membranes were washed 3 more times in TBS-T then visualized by chemiluminescence using ECL-select (GE-Healthcare). Chemiluminescence was detected using Bio-Rad blot scanner and densitometry was determined using ImageJ. Membranes were stripped in ReBlot Plus Mild Antibody Stripping Solution (Sigma) at room temperature for 20 min, and re-probed for tubulin as a loading control. Band intensities were normalized against tubulin loading controls, presented as fold change.

Cytoskeleton staining and analysis

Following monocyte isolation from human blood, cells were cultured in 0.5 mL of media as a density of 500,000 cells per mL onto 13 mm coverslips in 24-well plates and left to differentiate as above. hMDMs were fixed with 4% (v/v) formaldehyde for 10 min at room temperature and then maintained in PBS at 4°C. At this point all samples were blinded so that the microscopy and analysis were performed without knowledge of condition or donor being assessed. Coverslips were then removed onto parafilm and cells were washed with PBS then quenched with ammonium chloride for 10 min before being washed again. Cells were permeabilized with 0.1% (v/v) Triton X- diluted in PBS for 4 min. Coverslips were then stained with Fluorescein Isothiocyanate labeled Phalloidin (Sigma-Aldrich) for 20 min and washed with PBS and then water. Coverslips were mounted onto slides using Mowiol and kept in the dark for at least 24 h to dry and then until imaging. Images were taken using a Nikon Ti-E with CFI Plan Apochromat λ 20X, N.A.0.75 objective lens. Four fields of view per condition per donor were taken and analyzed using ImageJ software v2.9.0/1.53t. Each cell was manually drawn around and then area, circularity (shape descriptors) and mean gray value were measured. A circularity score of 1.0 indicates a perfect circle whereas values approaching 0.0 indicate an increasingly elongated shape. The median for area and circularity and geometric mean for mean gray value were then calculated for each image and an average was taken.

QUANTIFICATION AND STATISTICAL ANALYSIS

GraphPad Prism 9 software was used to generate all statistical analysis and graphs. N numbers and statistical analysis are stated for each experiment in the figure legends including the statistical test used, exact value of n and what n represents, definition of center and dispersion and precision measures. Differences were considered to be significant when p values were <0.05. Donors used in RNA sequencing were blinded prior to analysis. All macrophage samples used for microscopy were also blinded prior to imaging and analysis to prevent bias. Unless otherwise stated, six biological replicates were used for all experiments with each having three technical replicates. N = 6 donors for each condition was used for all experiments due to this being previously shown to give statistical power. Where possible, when comparing the same donor under different conditions, paired analysis was performed. ANOVA was used for time course experiments (Figure 1E; Figure 4D).

Cell Reports, Volume *43*

Supplemental information

Aging-related defects in macrophage function are driven by MYC and USF1 transcriptional programs

Charlotte E. Moss, Simon A. Johnston, Joshua V. Kimble, Martha Clements, Veryan Codd, Stephen Hamby, Alison H. Goodall, Sumeet Deshmukh, Ian Sudbery, Daniel Coca, Heather L. Wilson, and Endre Kiss-Toth

Supplementary Table 1 – Demographics of human donors

Age range	Mean age	Sex
18-30 years	23.7 ± 1.2 years	Female = 4, Male = 2
>50 years	60.5 ± 5.7 years	Female = 3, Male = 3

Age, sex and medication use were recorded. Ethnicity was not recorded as part of our ethics. Donors were excluded if they had an infection in the past 6 weeks, a vaccination in the past 2 weeks or if they were on medication altering immune function or statins.

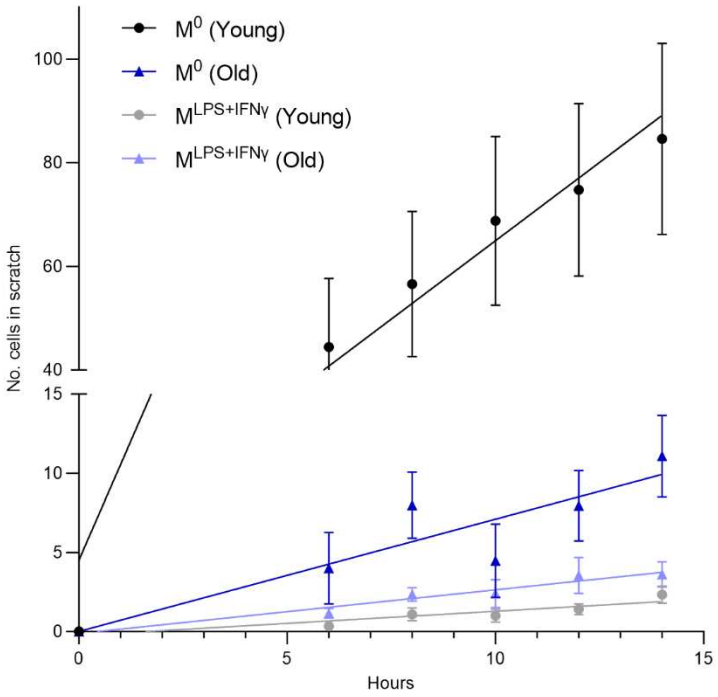

Supplementary Fig 1 – Motility of $M^{LPS+IFN\gamma}$ polarised human monocyte-derived macrophages

Number of MDMs returning to the scratch from young (22-25 years, N=6) and older (54-71 years, N=6) human subjects over 14 hours, with data being collected at 0, 6, 8, 10, 12 and 14 hours after the scratch was drawn. Data are presented as mean ± SEM with each datapoint representing the mean of six donors, with three fields of view taken per donor for each condition. MDMs were differentiated from human blood for 7 days in M-CSF and then either left unstimulated (M^0) or further polarised for 24 hours with LPS and IFNγ ($M^{LPS+IFN\gamma}$).

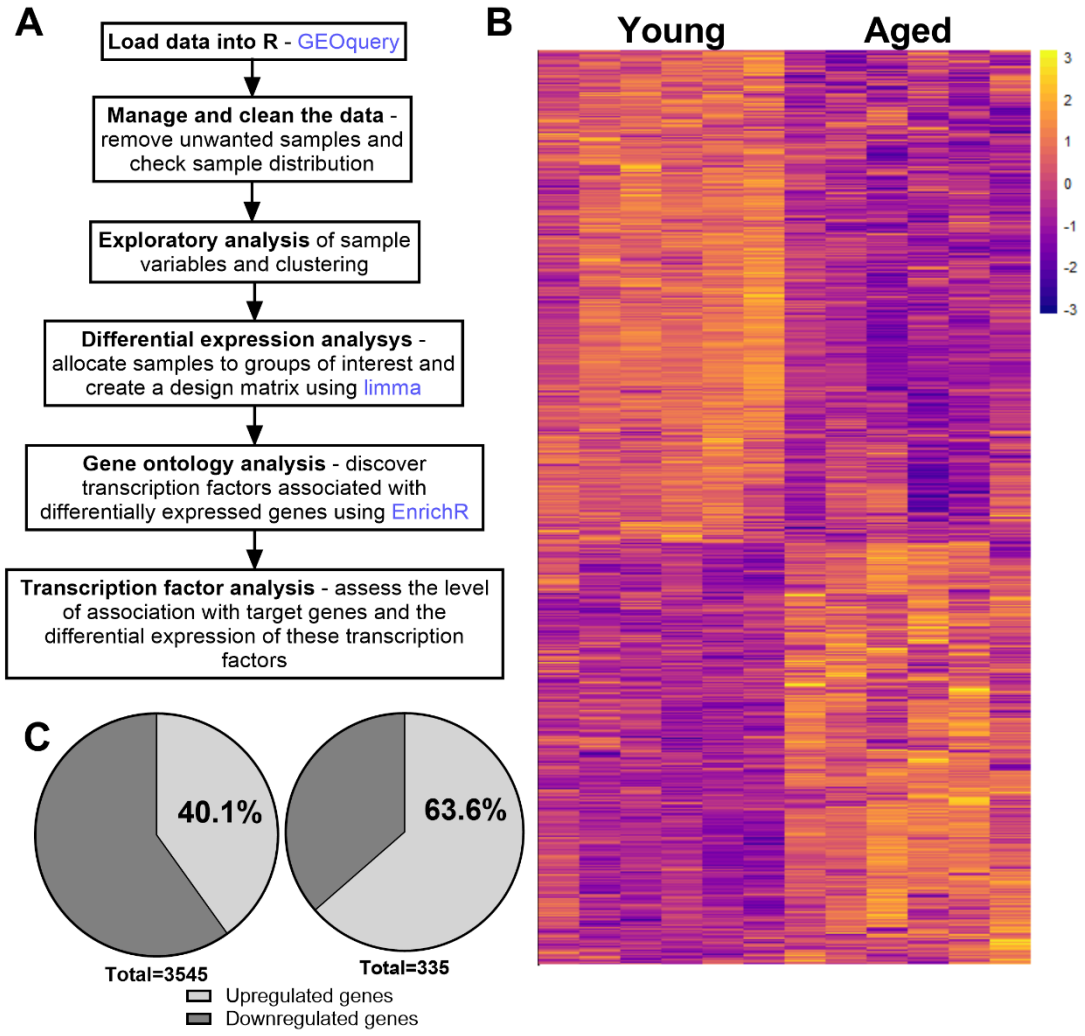

Supplementary Fig 2 – Age-related differentially expressed genes in mouse alveolar macrophages

A. Main steps in the pipeline for published microarray dataset GSE84901 analysis. Boxes represent the overall objectives, blue text shows the packages used.

B. A total of 3,545 genes were differentially expressed with age LogFC > 1, P value < 0.05.

C. Of these differentially expressed genes, 1,422 (40.1%) were upregulated and 2,123 (59.9%) were downregulated with age. Increasing the threshold of differential expression to LogFC > 1.5 and P value < 0.05, 213 genes (63.3%) were upregulated and 122 genes (36.4%) were downregulated with age.

Supplementary Table 2 – USF1 and MYC discrete signals from Phenoscanner

Data for 9 discrete (r2<0.3) eQTL signals for *USF1* and 1 for *MYC* were extracted from Phenoscanner. All eQTL data is from whole blood. SNP marker (rsid), chromosome and position (hg38), effect allele (EA) and frequency (EAF, Eur) is shown alongside position in relation to the gene, source study, P-value and the direction of effect associated with the effect allele. Study: eQTLGen Consortium phase 1, N = 31,684; BIOSQTL, N = 2,116; Joehanes R, N = 5,257.

Gene	Signal	SNP	Chromosome: position	EA	EAF	Position	Study	P	Direction	Tissue
USF1	1	rs147573079	chr1:161039365	A	0.0129	3_prime_UTR	eQTLGen	3.06E-11	-	Whole blood
		rs75089506	chr1:161044519	A	0.0129	intron	eQTLGen	2.99E-11	-	
USF1	2	rs3737787	chr1:161039733	A	0.2942	3_prime_UTR	BIOSQTL	6.65E-46	+	Whole blood
		rs2073658	chr1:161040972	T	0.2942	intron	BIOSQTL	5.35E-46	+	
		rs2073656	chr1:161041565	C	0.2942	intron	BIOSQTL	5.35E-46	+	
		rs2073655	chr1:161042800	A	0.2942	intron	BIOSQTL	5.35E-46	+	
USF1	3	rs2516841	chr1:161040984	A	0.2386	intron	eQTLGen	2.1E-285	-	Whole blood
		rs2774276	chr1:161041926	C	0.7614	intron	eQTLGen	2.5E-286	+	
		rs2073657	chr1:161041001	T	0.6282	intron	BIOSQTL	1.1E-203	+	
		rs2516839	chr1:161043331	T	0.6292	5_prime_UTR	BIOSQTL	7.6E-207	+	
		rs2774273	chr1:161044195	C	0.6292	intron	BIOSQTL	7.6E-207	+	
		rs2516837	chr1:161044937	A	0.3708	5_prime_UTR	BIOSQTL	2.4E-207	-	
USF1	4	rs17221763	chr1:161041419	A	0.0219	splice_region	eQTLGen	5.17E-35	-	Whole blood
		rs17175575	chr1:161041525	T	0.0229	intron	eQTLGen	4.09E-36	-	
USF1	5	rs2516840	chr1:161041527	A	0.2694	intron	eQTLGen	4.9E-119	-	Whole blood
USF1	6	rs2073653	chr1:161042970	T	0.8678	intron	eQTLGen	1.1E-122	+	Whole blood
		rs6686076	chr1:161043522	T	0.8678	intron	eQTLGen	8.4E-123	+	
		rs6427572	chr1:161043813	A	0.1332	intron	eQTLGen	1.1E-112	-	
		rs1556260	chr1:161044656	T	0.1322	intron	eQTLGen	1.2E-122	-	
		rs1556259	chr1:161044859	A	0.8678	intron	eQTLGen	9.6E-123	+	
USF1	7	rs149397699	chr1:161044634	T	0.9791	intron	eQTLGen	7.4E-26	+	Whole blood
MYC	1	rs2070583	chr8:127741008	A	0.9821	3_prime_UTR	Joehanes R	2.09E-08	-	Whole blood

Supplementary table 3 – Genome wide associations with sentinels for 10 *USF1* associations from OpenTargets

SNP	Trait	Trait Category	P-value	Beta	PMID	Author	N
rs12116949	Monocyte percentage of white blood cells	Measurement	9.80E-23	0.0228015	32888494	Vuckovic D	408112
	Monocyte count	Measurement	2.57E-16	0.016888	32888493	Chen MH	521594
	Monocyte percentage	Measurement	8.08E-11	0.0453607		UKB Neale v2	349861
	Mean platelet volume	Measurement	3.92E-10	-0.013118	32888493	Chen MH	460935
	Platelet distribution width	Measurement	7.21E-10	-0.00828198		UKB Neale v2	350470
	Mean platelet volume	Measurement	7.10E-09	-0.0129142	32888494	Vuckovic D	408112
	Platelet distribution width	Measurement	3.30E-08	-0.0129789	32888494	Vuckovic D	408112
rs2774276	Monocyte count	Measurement	4.40E-22	0.020875	32888493	Chen MH	521594
	Monocyte count	Measurement	2.70E-14	0.0167299	34226706	Barton AR	443529
	Lymphocyte counts	Measurement	2.16E-10	0.013872	32888493	Chen MH	524923
	Monocyte percentage of white blood cells	Measurement	1.50E-09	0.0148253	32888494	Vuckovic D	408112
	Lymphocyte counts	Measurement	5.00E-08	0.0133554	32888494	Vuckovic D	408112
rs2516840	Monocyte count	Measurement	4.00E-08	0.011392	32888493	Chen MH	521594

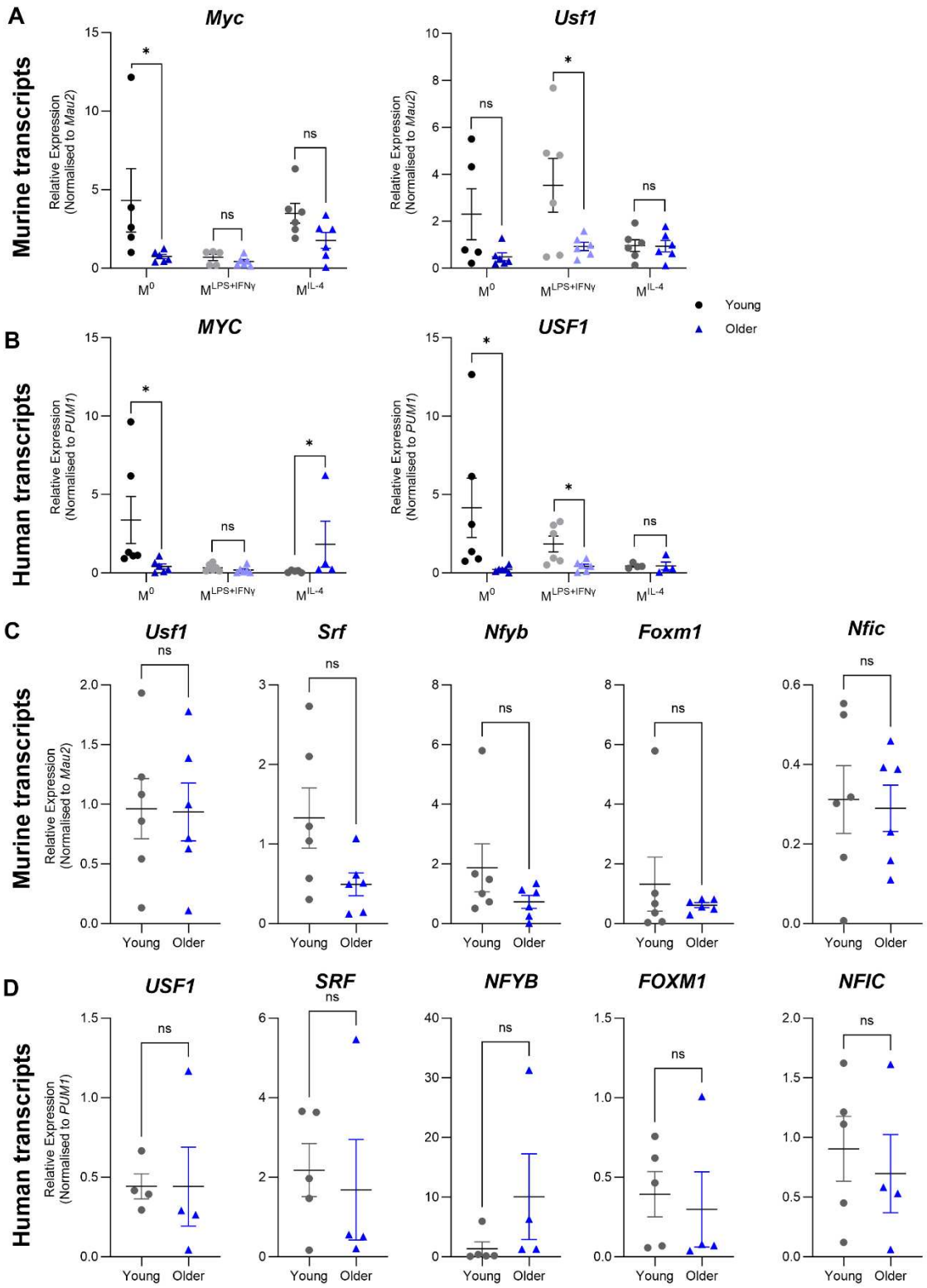

Supplementary Fig 3 – Expression of transcription factors with age in murine bone marrow-derived macrophages and human monocyte-derived macrophages polarised towards different phenotypes

A. Age-related changes in expression of *Myc* and *Usf1* in bone marrow derived macrophages isolated from young (2-5 months, N=6) and aged (22-24 months, N=6) C57BL/6J mice. *Mau2* expression was used as an internal control.

B. Age-related changes in expression of *MYC* and *USF1* in monocyte derived macrophages isolated from young (22-25 years, N=6) and older (54-71 years, N=6) healthy human donors. *PUM1* expression was used as an internal control.

C. Age-related changes in expression of transcription factors in bone marrow-derived macrophages isolated from young (2-5 months, N=6) and old (22-24 months, N=6) C57BL/6J mice. *Mau2* expression was used as a housekeeping control.

D. Age-related changes in expression of transcription factors in monocyte-derived macrophages isolated from young (22-25 years, N=4-5) and older (54-71 years, N=4) healthy human donors. *PUM1* expression was used as a housekeeping control.

Data are presented as mean ± SEM with each datapoint representing an individual mouse or human donor, that is the mean of three technical replicates. M^0 – cells left unstimulated, $M^{LPS+IFN\gamma}$ – cells stimulated with LPS and IFNγ for 24 hours, $M^{IL\text{-}4}$ – cells stimulated with IL-4 for 24 hours. Mann-Whitney test, * $P < 0.05$.

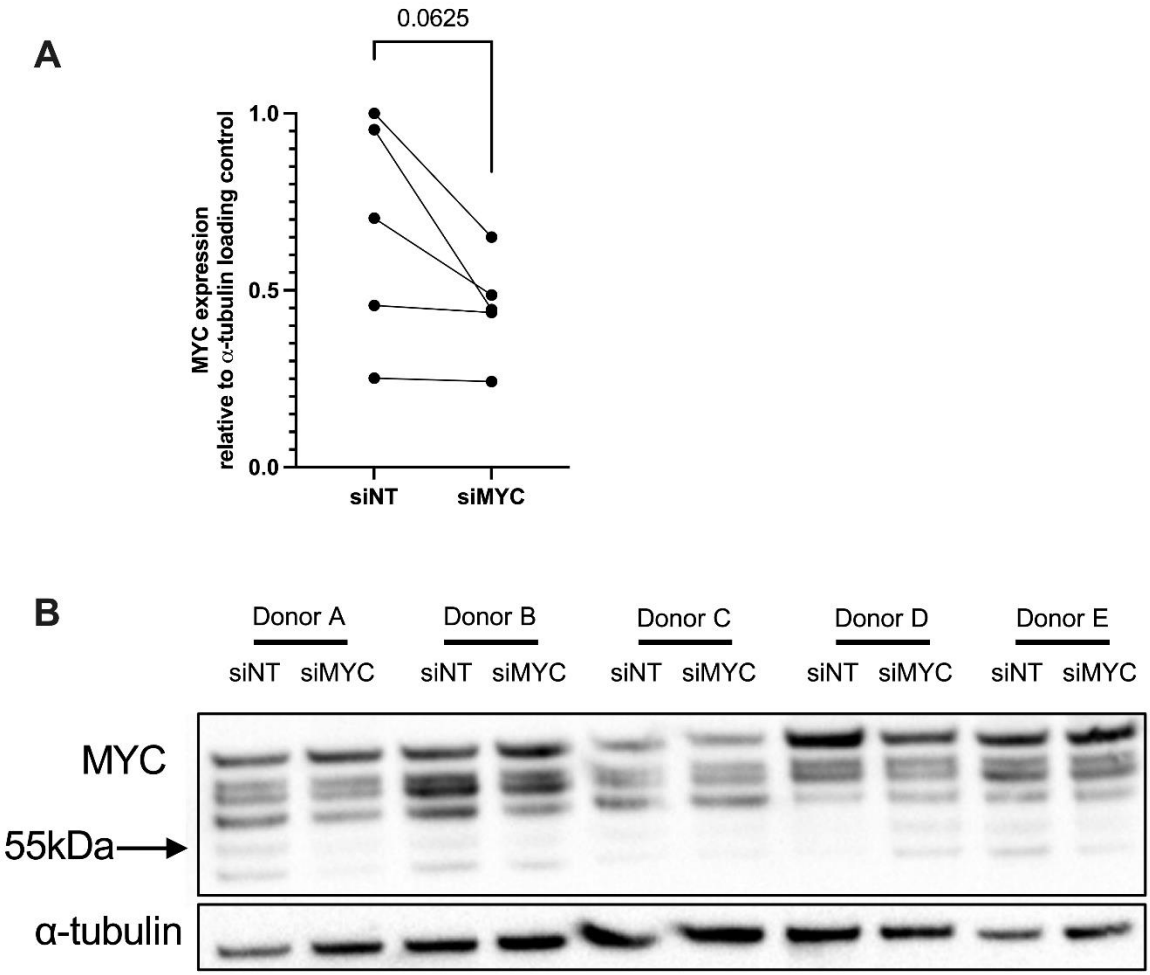

Supplementary Fig 4 – Immunoblotting for MYC in human MDMs isolated from 5 young donors with control (siNT) or MYC (siMYC) targeted siRNA knockdown

A. MYC expression quantified from total band density, normalised to α-tubulin loading control band density for each sample using ImageJ. Data are presented as mean ± SEM with each datapoint representing an individual donor. N=5, Wilcoxon matched-pairs signed rank test, P = 0.0625.

B. Immunoblots of human MDMs from 5 separate young donors used for quantification in A. Upper blot is anti-human-c-MYC, molecular weight 51kDa; all bands were used in quantification since c-MYC undergoes phosphorylation, ubiquitination, O-linked glycosylation, and acetylation. Lower blot is anti-α-tubulin used as loading control.

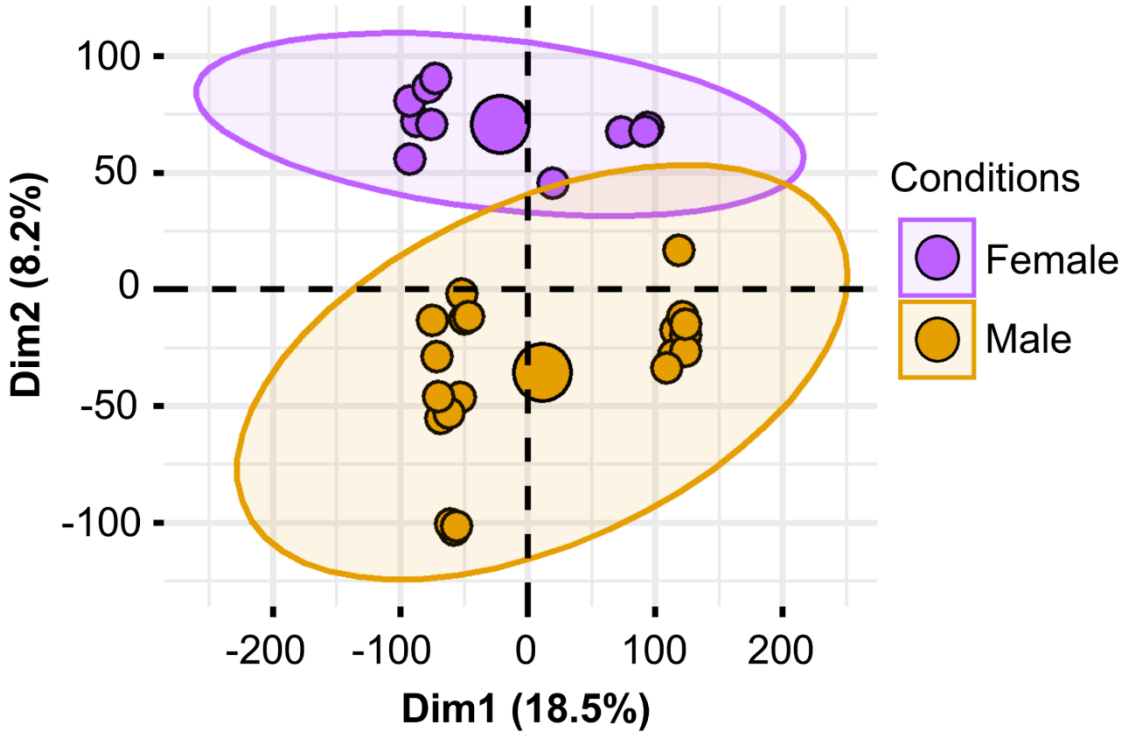

Supplementary Fig 5 – Macrophage phenotype and donor sex cause the largest variance in samples for RNA sequencing analysis

Principal component analysis of all samples highlighting the first two dimensions accounting for variability between samples. This was done using factoextra package in R.

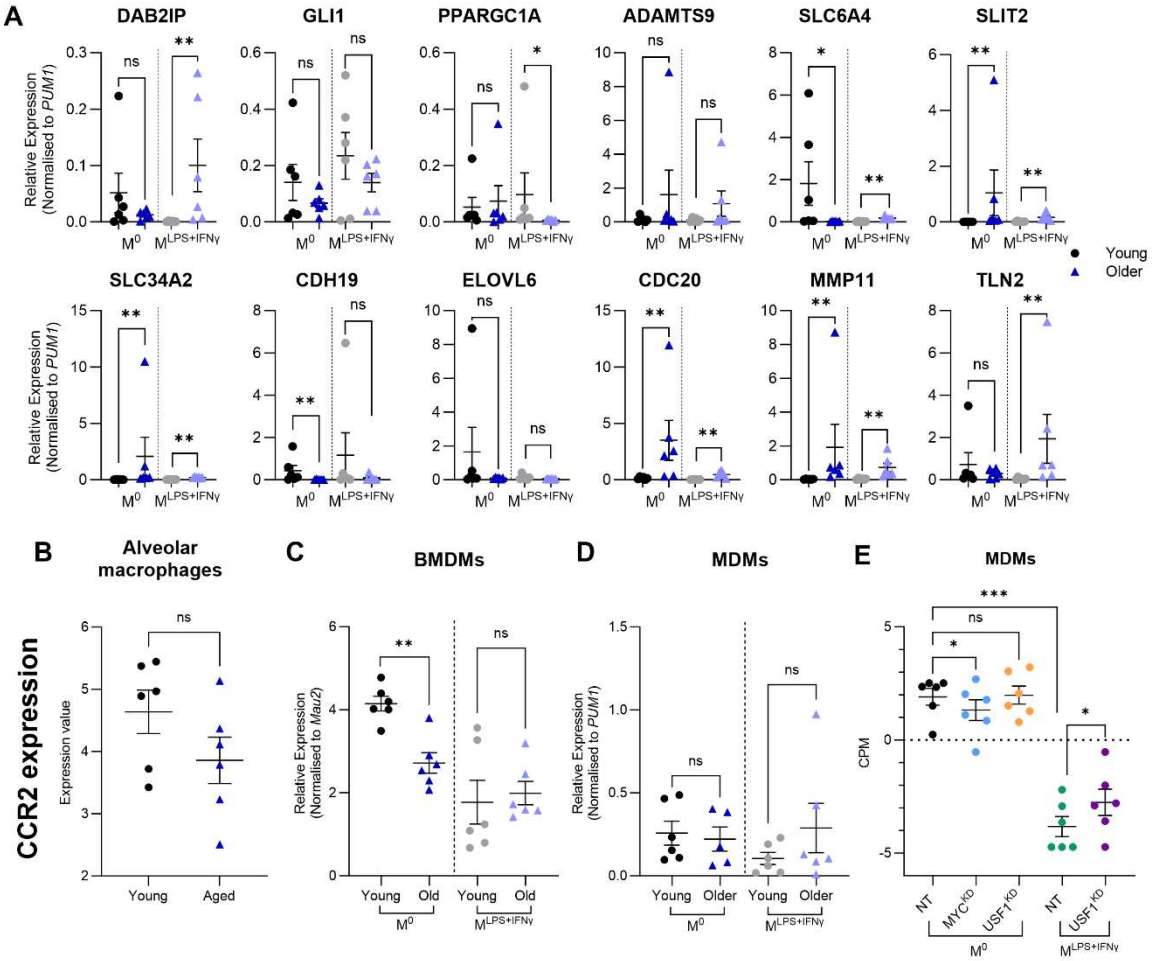

Supplementary Fig 6 – Age-related changes in expression of key genes associated with macrophage function in different macrophage populations

A. Age-related changes in expression of selected genes in monocyte derived macrophages isolated from young (22-25 years, N=6) and older (54-71 years, N=6) healthy human donors. These genes were selected from transcription factor knockdown RNA sequencing comparisons. *PUM1* expression was used as an internal control. Data are presented as mean ± SEM with each datapoint representing an individual donor that is the mean of three technical repeats. M^0 – cells left unstimulated, $M^{LPS+IFN\gamma}$ – cells stimulated with LPS and IFNγ for 24 hours. N = 6, Mann-Whitney test. * P < 0.05, ** P < 0.01.

B. Age-related changes in *Ccr2* expression in murine alveolar macrophages isolated from young (2-4 months, N=6) and aged (22-24 months, N=6) C57BL/6 mice via microarray analysis. N=6, Mann-Whitney test.

C. Age-related changes in *Ccr2* expression in bone marrow-derived macrophages isolated from young (2-5 months, N=6) and old (20-22 months, N=6) C57BL/6 mice via RT-qPCR. BMDMs were differentiated for 5 days with M-CSF and left unstimulated of further stimulated with LPS and IFNγ for 24 hours. *Mau2* expression was used as an internal control. Data are presented as mean ± SEM with each datapoint representing an individual donor that is the mean of three technical repeats. M^0 – cells left unstimulated, $M^{LPS+IFN\gamma}$ – cells stimulated with LPS and IFNγ for 24 hours. N=6, Mann-Whitney test, ** P < 0.01.

D. Age-related changes in *CCR2* expression in monocyte-derived macrophages isolated from young (22-25 years, N=6) and older (54-71 years, N=6) healthy human donors via RT-qPCR. MDMs were differentiated for 7 days with M-CSF and left unstimulated or further stimulated with LPS and IFNγ for 24 hours. *PUM1* expression was used as an internal control. Data are presented as mean ± SEM with each datapoint representing an individual donor that is the mean of three technical repeats.

M^0 – cells left unstimulated, $M^{LPS+IFN\gamma}$ – cells stimulated with LPS and IFNγ for 24 hours. N=6, Mann-Whitney test.

E. Relative expression of *CCR2* after *MYC* or *USF1* knockdown in young human monocyte-derived macrophages via RNA sequencing analysis. MDMs were differentiated for 7 days with M-CSF and stimulated with siRNA for 72 hours. Data are presented as mean ± SEM with each datapoint representing an individual donor that is the mean of three technical repeats. M^0 – cells left unstimulated, $M^{LPS+IFN\gamma}$ – cells stimulated with LPS and IFNγ for 24 hours. N=6, One-way ANOVA with Sidaks multiple comparison, * $P < 0.05$, *** $P < 0.001$

Supplementary Table 4 – Oligonucleotide sequences for RT-qPCR of human (Rows 1-36) and murine (Rows 37-44) samples

No.	Target gene	Forward primer (5'-to-3')	Reverse primer (5'-to-3')
1	PUM1	GCATTTGGACAAGGTCTGGCAG	GCTACAAGTCGAACAGGAGCTC
2	MYC	AGAGTTTCATCTGCGACCCG	GAAGCCGCTCCACATACAGT
3	USF1	GCTCTATGGAGAGCACCAAGTC	AGACAAGCGGTGGTTACTCTGC
4	NFYB	GGAATTGGTGGAGCAGTCACAG	CCGTCTGTGGTTATTAAGCCAGC
5	SRF	TCACCTACCAGGTGTCGGAGTC	GTGCTGTTTGGATGGTGGAGGT
6	FOXM1	TCTGCCAATGGCAAGGTCTCCT	CTGGATTCGGTCGTTTCTGCTG
7	NFIC	TGGCGGCGATTACTACACTTCG	GGCTGTTGAATGGTGACTTGTCC
8	ATP8B1	CTTCTTGCTCGCAGTTTGCCAC	GCCAAAGTTCCTGGCAGCGTTT
9	SFRP4	CTATGACCGTGGCGTGTGCATT	GCTTAGGCGTTTACAGTCAACATC
10	GDF1	GTCACCCTGCAACCGTGCCAC	AGGTCGAAGACGACTGTCCACT
11	STAB2	ACTGGCTCCTTACCAAACCTGC	GAGCAAACACTGTGTAGGCATCG
12	MMP8	CAACCTACTGGACCAAGCACAC	TGTAGCTGAGGATGCCTTCTCC
13	PLOD2	GACAGCGTTCTCTTCGTCCTCA	CTCCAGCCTTTTCGTGGTGACT
14	ITGB6	TCTCCTGCGTGAGACACAAAGG	GAGCACTCCATCTTCAGAGACG
15	ITGA2B	CTGTCCAGCTACTGGTGCAAGA	ATGTTGTGCCCAGTGGCTCCAA
16	CDH8	AACGCTGGCAACACCACTTGAC	GCGTTGTCATTGACATCCAGCAC
17	ADAMTS9	CCATTCAGAGGTGCAGTGAGTTC	ACCAGACCTGGCGGTGCTTATG
18	AJUBA	AGCCACCAGGTCCTTTCGTTCC	GGCATTGCTCTGCCCATAGATG
19	CDH19	ATTGGTCAGCCAGGAGCGTTGT	GCAGATTCAGAGACAGTCAAGCG
20	ANGPTL3	CCTGAAACTCCAGAACACCCAG	TTCCACGGTCTGGAGAAGGTCT
21	PCDHGB4	CAACACGGACTGGCGTTTCTCT	GATCATGGCTTGCAGCATCTCTG
22	DAB2IP	TCATCGCCAAGGTCACCCAGAA	CGCTGCATGTTGGTCCACTCAT
23	GLI1	AGCCTTCAGCAATGCCAGTGAC	GTCAGGACCATGCACTGTCTTG
24	PPARGC1A	CCAAAGGATGCGCTCTCGTTCA	CGGTGTCTGTAGTGGCTTGACT
25	SLC6A4	TCACAGTGCTCGGTTACATGGC	GAAAGTGGACGCTGGCATGTTG
26	SLIT2	CAGAGCTTCAGCAACATGACCC	GAAAGCACCTTCAGGCACAACAG
27	SLC34A2	CGTGTGTGCATGGGTCAAAG	CAATCTTGCTGCACGGCTAC
28	ELOVL6	CCATCCAATGGATGCAGGAAAAC	CCAGAGCACTAATGGCTTCCTC
29	CDC20	CGGAAGACCTGCCGTTACATTC	CAGAGCTTGCACTCCACAGGTA
30	MMP11	GAGAAGACGGACCTCACCTACA	CTCAGTAAAGGTGAGTGGCGTC
31	MMP13	GCACTTCCCACAGTGCCTAT	AGTTCTTCCCTTGATGGCCG
32	TLN2	CAAGGAAGTCGCCAACAGCACT	TTGAGGCGAACGCTGTCAGGTT
33	ITGB1BP2	GACCACACTGTGCTGAGAAGCT	AGCAGCTTCAGAGGCAACTCTG
34	WNT11	CTGTGAAGGACTCGGAACTCGT	AGCTGTCGCTTCCGTTGGATGT
35	GPR32	CTGGGGCCCTTAGCAATCAT	AGATGGACCAACAGCACCAC
36	CCR2	GGGATGACTCACTGCTGCAT	TGCTTTCGGAAGAACACCGA
37	Mau2	TGGTTACCTGGAGAAGGCACAG	ATGCTCCAGCAGGATCACTTGG
38	Myc	TTGAAGGCTGGATTTCCTTTGGGC	TCGTCGCAGATGAAATAGGGCTGT
39	Usf1	CGTCTTCCGAACTGAGAATGGG	CTGGGTCATAGACTGAGTGGCA
40	Nfyb	ACCAAACAGCCGATTGGAGA	CTAGCTGGGAGGCATCTGTG
41	Srf	CACCTACCAGGTGTCGGAAT	GTCTGGATTGTGGAGGTGGT
42	Foxm1	GTCTCCTTCTGGACCATTCACC	GCTCAGGATTGGGTCGTTTCTG
43	Nfic	TGACTCAGTAAGTTCGGCGG	GTTGAACCAGGTGTAGGCGA
44	Ccr2	GCTGTGTTTGCCTCTCTACCAG	CAAGTAGAGGCAGGATCAGGCT